

# Estimation of surface upward longwave radiation from MODIS and VIIRS clear-sky data in the Tibetan Plateau

Zhonghu Jiao <sup>a</sup>, Guangjian Yan <sup>a,\*</sup>, Jing Zhao <sup>a</sup>, Tianxing Wang <sup>b</sup>, Ling Chen <sup>c</sup>

<sup>a</sup> State Key Laboratory of Remote Sensing Science, School of Geography, Beijing Normal University, Beijing 100875, China

<sup>b</sup> Institute of Remote Sensing and Digital Earth, Chinese Academy of Sciences, Beijing 100101, China

<sup>c</sup> The Academy of Forestry, Beijing Forestry University, Beijing 100083, China



## ARTICLE INFO

### Article history:

Received 2 August 2014

Received in revised form 29 January 2015

Accepted 20 February 2015

Available online 16 March 2015

### Keywords:

Surface upward longwave radiation

MODIS

VIIRS

Tibetan Plateau

Artificial Neuron Network (ANN)

## ABSTRACT

Surface upward longwave radiation (SULR) is one critical component of the surface energy balance and is closely related to the surface temperature fields. The SULR with the moderate spatial resolution and appropriate precision in the Tibetan Plateau, a large and complex cryosphere, can enhance our understanding of the land surface processes, atmospheric circulations and even global climate change. The purpose of this paper is to estimate SULR from top-of-atmosphere (TOA) radiances of Moderate Resolution Imaging Spectroradiometer (MODIS) and Visible Infrared Imaging Radiometer Suite (VIIRS). A hybrid method is proposed that combines extensive radiative transfer simulation and the Artificial Neuron Network (ANN) statistical model. For the sake of ensuring the availability of the simulation database, the eligible profiles from MODIS atmospheric profiles product were screened according to five criteria. And then the analyses on the important parameters of the simulation dataset were performed to check the integrality of this dataset. Moreover, the variables' importance was analyzed, and TOA radiances of MODIS channels 29, 31, 32 and 33 (or VIIRS channels M14, M15 and M16) and sensor view zenith angle (VZA) were selected to retrieve SULR. The ANN-based retrieval model was created finally based on this simulation dataset. The evaluation showed good agreements for both MODIS and VIIRS training and testing datasets with  $R^2$  greater than 0.98. The MODIS SULR was validated using two-year ground-measured data at seven sites in the Tibetan Plateau with  $R^2$  of 0.886, root-mean-square error (RMSE) of 26.985  $\text{W m}^{-2}$  and mean bias error (MBE) of 10.812  $\text{W m}^{-2}$  as a whole. And the relevance was obvious from the overall trend and distribution though the discrepancy was relatively large when directly comparing SULR from VIIRS and MODIS data. The validation results showed that the ANN model is a good nonlinear model to retrieve SULR with the TOA radiances and VZA.

© 2015 Elsevier Inc. All rights reserved.

## 1. Introduction

The Tibetan Plateau, known as the “Third Polar”, is the large highland core of Asia with an average elevation of over 4500 m (Qiu, 2008). This complex cryosphere significantly influences climate and environment of the East and South Asia as well as mankind resides there (Wonsick & Pinker, 2013). This unique region is also sensitive to water cycles and global climate changes, thus can be a good indicator to investigate what happened to the system of the Earth (Yang et al., 2014). The surface radiation balance (SRB) is an important component within it (Shi & Liang, 2013; Yang, Koike, Stackhouse, Mikovitz, & Cox, 2006).

Surface radiation balance includes net longwave and shortwave radiative fluxes, which are the critical driving factors in models of numerical weather forecasting, hydrology, ecology, etc. SRB is also the essential parameter in the energy exchanges between the land surface and atmosphere, thus thoroughly impacts climate and land cover changes (Soci, Fischer, & Horányi, 2006). As a significant part of the SRB, surface longwave radiation plays an essential role in the surface material and energy cycle, particularly in the night, high altitude and polar regions. The surface longwave radiation consists of three components: upward, downward and net radiation. Surface upward longwave radiation (SULR) mainly represents the capability of thermal radiation from the Earth's surface and is related to the solar radiation, evapotranspiration, soil moisture, land cover types and topography. Accurate retrieval of SULR is important for investigating the spatiotemporal variability of SULR on regional and global scales, thus has high scientific and practical merits.

SULR (4–100  $\mu\text{m}$ ) is the total upward component of the thermal infrared radiative flux at the Earth's surface in  $\text{W m}^{-2}$ , which is the

\* Corresponding author.

E-mail address: [gjyan@bnu.edu.cn](mailto:gjyan@bnu.edu.cn) (G. Yan).

sum of surface emitted thermal radiation and the first-order reflected component of surface downward longwave radiation (SDLR) as follows:

$$\text{SULR} = \varepsilon\sigma T^4 + (1-\varepsilon)\text{SDLR}, \quad (1)$$

where  $\sigma$  is the Stefan–Boltzmann constant;  $\varepsilon$  is the surface broadband emissivity; and  $T$  is the surface skin temperature (K). According to the Kirchhoff's law and conservation of energy, the surface broadband albedo is equal to one minus the broadband emissivity. SDLR is the total downward thermal radiative flux density emitted by the atmosphere and clouds that reaches the earth's surface. SULR is dominated by the thermal inertia of the land or ocean (Mlynaczak, Smith, Wilber, & Stackhouse, 2011), and is the main cause of surface cooling in the clear night (Helbig & van Herwijken, 2012).

SULR can be retrieved according to its definition in Eq. (1), which can be called the temperature-emissivity method (Long, Gao, & Singh, 2010; Wang et al., 2005; Wang, Liang, & Augustine, 2009). The surface skin temperature and emissivity data can be derived from the satellite data, like Moderate Resolution Imaging Spectroradiometer (MODIS) products. SDLR can be obtained from ground-measured data, reanalysis data or results simulated by radiation transfer models (Abramowitz, Pouyanné, & Ajami, 2012; Nussbaumer & Pinker, 2012).

Hybrid method is a physical-based retrieval approach to estimate SULR from satellite data. Firstly, extensive simulation database is established by radiation transfer codes, which includes SULR, top-of-atmosphere (TOA) radiances or brightness temperatures of a multispectral satellite sensor and various key variables associated with the different surface properties (such as surface emissivity, skin temperature) and atmospheric conditions (air temperature, water vapor content etc.). Secondly, SULR is derived using statistical regression analysis, like linear methods (Wang & Liang, 2010; Wang et al., 2009) or nonlinear methods (Wang et al., 2009; Wang, Yan, & Chen, 2012). The results of Wang et al. (2009) shows that the root-mean-square error (RMSE) of the hybrid method using the Artificial Neuron Network (ANN) model is smaller than linear models, indicating the advantage of nonlinear models.

Generally, all of the biases and limits of data products affect the final SULR. Temperature-emissivity method requires data products of surface skin temperature, emissivity and SDLR. However, the state-of-art products estimated from remotely sensed data still have great uncertainty (Wang & Liang, 2009). Narrowband emissivity data have to be converted to the broadband emissivity (Ren, Liang, Yan, & Cheng, 2013; Wang et al., 2005). The anisotropy of the surface emissivity retrieved from satellite images can further aggravate this uncertainty (Ren, Yan, Chen, & Li, 2011; Ren et al., 2014). In addition, SDLR is not a ready-made data: ground-measured data usually mismatch with satellite data; and reanalysis data always have coarser spatial resolution. There are many input parameters in Wang's model which used the hybrid method, such as air and dew point temperature profiles (Wang et al., 2012). These parameters may bring in more uncertainties than the increased accuracy to the estimated SULR. Therefore, more input variables don't always mean higher accuracy.

**Table 1**  
The band characteristics of MODIS and VIIRS data.

| Sensor | Band number | Band range ( $\mu\text{m}$ ) | NE $\Delta$ T (K) | Nadir resolution (m) |
|--------|-------------|------------------------------|-------------------|----------------------|
| MODIS  | 29          | 8.400–8.700                  | 0.05              | 1000                 |
|        | 31          | 10.780–11.280                | 0.05              |                      |
|        | 32          | 11.770–12.270                | 0.05              |                      |
|        | 33          | 13.185–13.485                | 0.25              |                      |
| VIIRS  | M14         | 8.4–8.7                      | 0.091 (270 K)     | 750                  |
|        | M15         | 10.26–11.26                  | 0.070 (300 K)     |                      |
|        | M16         | 11.54–12.49                  | 0.072 (300 K)     |                      |

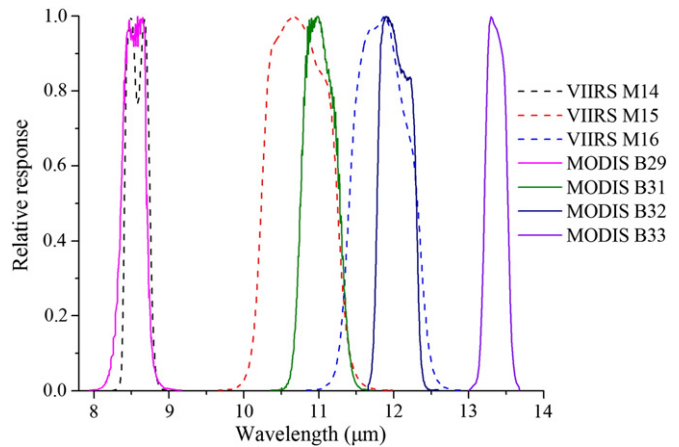


**Fig. 1.** The spectral response functions of MODIS channels 29, 31, 32 and 33, and VIIRS channels M14, M15 and M16.

Currently, there are various global surface longwave radiation products retrieved from remote sensing data, such as International Satellite Cloud Climatology Project dataset (ISCCP-FD) (Zhang, Rossow, Lacis, Oinas, & Mishchenko, 2004), Global Energy and Water Exchanges Project (GEWEX) surface radiation budget dataset (Pinker & Laszlo, 1992), Clouds and Earth's Radiant Energy System (CERES) dataset (Kato et al., 2013) and the Satellite Application Facility on Climate Monitoring (CM-SAF) (Schulz et al., 2009) data products of the European Organization for the Exploitation of Meteorological Satellites (EUMETSAT). In addition, there are many reanalysis products including SULR, like Climate Forecast System Reanalysis (CFSR) of the National Centers for Environmental Prediction (NCEP), NASA's Modern Era Retrospective Analysis for Research and Application (MERRA), Interim Reanalysis (ERA-Interim), and Japanese 55-year Reanalysis (JRA-55). These available products are designed for large-scale models, which always have high temporal resolution (1–3 h), but generally low spatial resolution (38 km to 2.5°). So they cannot satisfy the requirements of many applications, like high-resolution (about 1–5 km) forecast systems, mesoscale land surface or environmental models (Guan, Tremblay, Isaac, Strawbridge, & Banic, 2000; Masson, Champeaux, Chauvin, Meriguet, & Lacaze, 2003). In heterogeneous areas or mountainous terrains, the surface longwave radiation is more significantly variable and the high-resolution (about 1 km) radiation data are preferred. Furthermore, acceptable precision of the retrieved instantaneous surface radiation from satellite data is less than 20 W m<sup>-2</sup>, monthly mean value is less

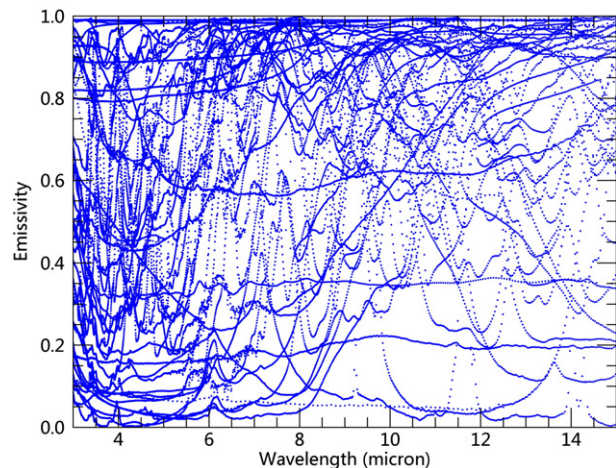


**Fig. 2.** Spectral emissivity curves used in the MODTRAN simulation from ASTER, UCSB and MODTRAN spectral libraries.

**Table 2**

Details of seven stations in the Tibetan Plateau.

| Number | Site name   | Land cover                            | Latitude<br>(°N) | Longitude<br>(°E) | Elevation<br>(m) |
|--------|-------------|---------------------------------------|------------------|-------------------|------------------|
| 1      | D105        | Sparse plateau meadow                 | 33.06429         | 91.94256          | 5038.6           |
| 2      | Amdo        | Prairie                               | 32.24096         | 91.62493          | 4695.2           |
| 3      | NPAM/MS3478 | Plateau meadow                        | 31.92623         | 91.71468          | 4619.5           |
| 4      | BJ (Bujiao) | Sand                                  | 31.36871         | 91.89518          | 4509.2           |
| 5      | Namco       | Alpine meadow                         | 30.77            | 90.99             | 4730             |
| 6      | LinZhi      | Plateau meadow surrounded by woodland | 29.77            | 94.74             | 3327             |
| 7      | ZhuFeng     | Bare land                             | 28.365           | 86.94806          | 4276             |

than  $10 \text{ W m}^{-2}$  for meteorological research (Ellingson, 1995; Gupta, Kratz, Wilber, & Nguyen, 2004), and  $5\text{--}10 \text{ W m}^{-2}$  for longwave radiation at 25–100 km spatial resolution (Wang et al., 2009). It is highly valuable of retrieving surface longwave radiation components from space with about 1 km spatial resolution and appropriate accuracy, which are not available yet.

In this paper, we propose a hybrid method combining with the MODerate resolution atmospheric TRANsmision (MODTRAN) radiative transfer model and the ANN model. This method can directly utilize MODIS and Visible Infrared Imaging Radiometer Suite (VIIRS) TOA radiances to estimate SULR and can avoid the error propagation in the retrieving processes of surface skin temperature, emissivity products and SDLR. Unlike Wang's model (Wang et al., 2009), the sensor view zenith angle was used in the ANN model, which can calibrate the nonlinear relationship between SULR and the sensor's TOA radiances so offer the flexibility for arbitrary view zenith angles, based on the analyses of the variables' importance. MODIS data with 1 km spatial resolution have been used in the surface radiation retrieval widely. Whereas the thermal infrared data of VIIRS instrument with finer resolution of 750 m, the successor of MODIS, have not been employed in this field. It has similar channel characteristics as MODIS in thermal infrared windows, so the same retrieval scheme was adopted in our work.

The article is structured as follows: satellite data, emissivity library and ground-measured data are described in Section 2. Section 3

introduces the radiative transfer simulation based on MODTRAN, variable selection and the ANN training and retrieval method. The sensitivity analyses were performed to check the impacts of solar illumination, atmospheric profile quantity and spectral emissivity data on the radiative transfer simulation and ANN model in Section 4. In Section 5, results of retrieval and validation are presented. In addition, the statistical characteristic of the simulation database is also shown. Section 6 gives the conclusions.

## 2. Data

### 2.1. MODIS and VIIRS data

MODIS and VIIRS have similar features in many aspects: MODIS has mature data products that are valid and have been evaluated by researchers widely; VIIRS is the next-generation polar-orbiting sensor with a capability for global thermal mapping and has many improvements compared to MODIS. The MODIS was equipped on the Terra polar-orbiting satellite on Dec. 18, 1999 and Aqua on May 4, 2002. These instruments can acquire data in 36 spectral bands from 0.405 to  $14.385 \mu\text{m}$  with 2330 km swath width and can view the entire Earth's surface every one or two days (Barnes, Pagano, & Salomonson, 1998). The VIIRS instrument aboard the Suomi National Polar-orbiting Partnership (S-NPP) was launched on October 28, 2011, and provides continuity with MODIS (Cao et al., 2013). VIIRS is a multispectral scanning radiometer and collects visible and infrared imagery in 22 bands between  $0.4 \mu\text{m}$  and  $12 \mu\text{m}$ , which further enhances the capabilities of moderate-resolution imaging of the land, atmosphere and oceans. This offers a good opportunity to improve our understanding of the radiation budget of the atmosphere and terrestrial surface.

The specific spectral bands used in this work include MODIS bands 29, 31, 32 and 33, and VIIRS bands M14, M15 and M16. They have the similar channel characteristics (Table 1). It can be found that MODIS's band noise-equivalent temperature difference ( $\text{NEAT}$ , 0.05) are better than VIIRS's (0.070, 0.072 and 0.091) except MODIS band 33 with  $\text{NEAT}$  of 0.25, but VIIRS data have higher spatial resolution of 750 m at nadir in contrast with MODIS 1-km data. The spectral response function of MODIS band 29 is analogous to VIIRS band M14, and those of VIIRS bands M15 and M16 are wider than MODIS bands 31 and 32 (Fig. 1).

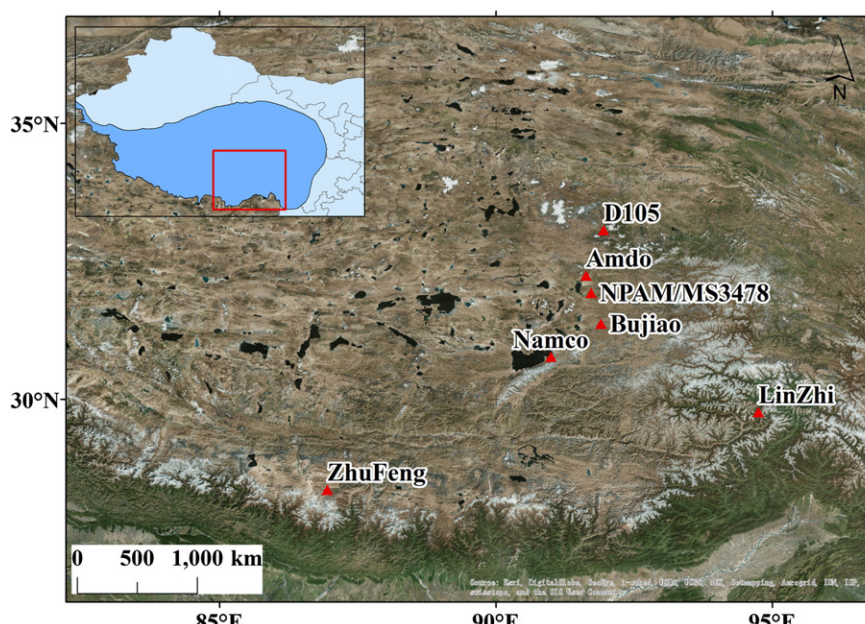


Fig. 3. The location of seven ground stations (red triangles) in the Tibetan Plateau. The background image is from Esri® Basemap gallery.

**Table 3**

The instrument information at the seven sites in the Tibetan Plateau.

| Number | Site names  | Instrument | Sampling interval (minutes) | Expected accuracy for daily totals (%) |
|--------|-------------|------------|-----------------------------|--|
| 1      | D105        | PIR        | 60                          | ±10                                    |
| 2      | Amdo        | PIR        | 30                          | ±6                                     |
| 3      | NPAM/MS3478 | PIR        | 60                          | ±10                                    |
| 4      | BJ(Bujiao)  | PIR        | 10                          | ±10                                    |
| 5      | Namco       | CNR-1      | 30                          | ±10                                    |
| 6      | LinZhi      | CNR-1      | 10                          | ±10                                    |
| 7      | ZhuFeng     | CNR-1      | 30                          | ±10                                    |

The MODIS products used in this study consist of MOD07/MYD07, MOD35\_L2, MOD021KM and MOD03 from MODIS Collection 6 data products, which include numerous improvements and changes. The detailed description and relevant documents of the algorithms can be found at [http://modis-atmos.gsfc.nasa.gov/products\\_C006update.html](http://modis-atmos.gsfc.nasa.gov/products_C006update.html). MOD07/MYD07 data are the atmospheric profiles products with 5 km spatial resolution, which consist of air temperature profile, dew point temperature profile, geopotential height profile, total column perceptible water vapor, surface temperature, surface elevation, and so on (Seemann, Li, Menzel, & Gumley, 2003). The profile has 20 fixed vertical atmospheric pressure levels, but the data in the highest four levels always have 100% relative humidity, which is unreasonable, so we removed them in the preprocessing phase. The MOD07 and MYD07 data were collected over the Tibetan Plateau in 2012 to establish the atmospheric profile database with the auxiliary data such as the surface elevation, skin temperature, time, etc. for each profile. MOD35\_L2 is the cloud mask product with 1 km spatial resolution indicating whether a pixel is blocked by the cloud or not. The pixels with confident clear or probably clear flag are considered as the clear-sky ones and the pixels with probably cloudy or cloudy flag are deemed as cloudy ones. MOD021KM is Level 1B at-aperture radiance dataset with 36 bands for each 1-km pixel. Four thermal infrared bands 29, 31, 32 and 33 were calibrated to radiance, geolocated and masked by the cloud mask. MOD03, the geolocation dataset, contains the solar zenith and azimuth angles, satellite zenith and azimuth angles, surface elevation, geodetic coordinates (the longitude and latitude information) and other auxiliary data with 1 km spatial resolution. It is mainly used to geolocate other data products above. In addition, satellite zenith angle data were extracted from MOD03 product as the input variable to estimate the SULR.

In this research, the employed VIIRS data products include VIIRS moderate resolution Sensor Data Records (SDR) product, VIIRS Cloud Mask (VCM) intermediate product and moderate bands SDR terrain corrected geolocation product. VIIRS moderate resolution SDR data are the sensor-measured TOA radiance/reflectance from M1 to M16

bands. We used only band M14, M15 and M16 radiance data that are within the thermal infrared atmospheric windows. VCM product provides the cloud mask data to identify the clear-sky or cloudy pixels. The pixels with medium or high cloud mask quality and confident clear or probably clear cloud detection results are considered as clear-sky pixels, and the others are cloudy pixels (Hutchison, Isager, & Hauss, 2011). Besides, geolocation product was used to geolocate other data products and to extract the sensor view zenith angle data.

## 2.2. Emissivity spectra

SULR is sensitive to the surface properties (or land cover types) that can be described by surface emissivity spectra. Therefore, emissivity spectra are the indispensable input data for the MODTRAN simulation. In theory, spectral emissivity library should contain spectra covered all possible surface types, but this is not practical indeed. So according to the representative land cover types (farm, bare-land, water, snow/ice, forest, etc.) in the Tibetan Plateau, a total 52 spectra were screened (Fig. 2) from MODTRAN software package, Advanced Spaceborne Thermal Emission and Reflection Radiometer (ASTER) (Baldridge, Hook, Grove, & Rivera, 2009) and UCSB (University of California, Santa Barbara) emissivity libraries based on the principle of maximum variance among emissivity data.

## 2.3. In situ measurements

The in situ radiation data at seven sites were used to validate the ANN-based retrieval model. The detailed information of the latitude, longitude, elevation and land cover about these seven stations is given in Table 2 and the geographic positions are shown in Fig. 3. They are all located at 3 to 5 km elevations and distributed at the Southeast of the Tibetan Plateau. The surface types include meadow, sand and bare land, etc. The data period spans from 2007 to 2008, with acceptable continuity despite some malfunctions resulted from the instrument itself or external environment. The instruments used to measure surface radiative fluxes, sample interval and instrument error at these sites are depicted in Table 3.

Two different kinds of radiometers are equipped in these ground stations. The CNR1 net radiometer by Kipp & Zonen contains a pyrgeometer facing upward and a downward complementary one, and measures the surface radiation budget about incoming atmospheric longwave radiation and surface outgoing longwave radiation (Michel, Philipona, Ruckstuhl, Vogt, & Vuilleumier, 2008). Pyrgeometer is in the spectral range from 5 to 50 μm. The Precision Infrared Radiometer (PIR) by Eppley Laboratory is intended for unidirectional measurements of incoming atmospheric and outgoing terrestrial radiative fluxes. The

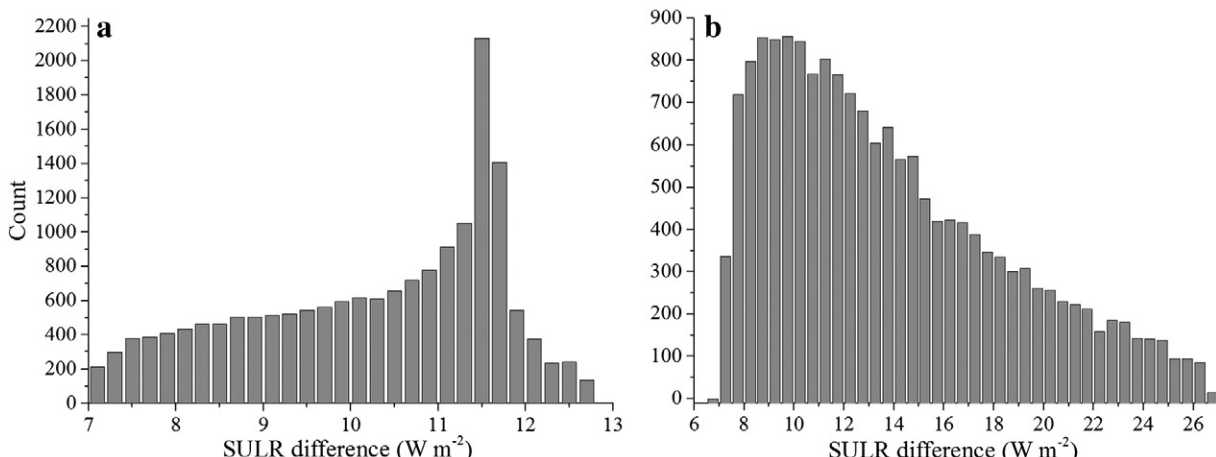
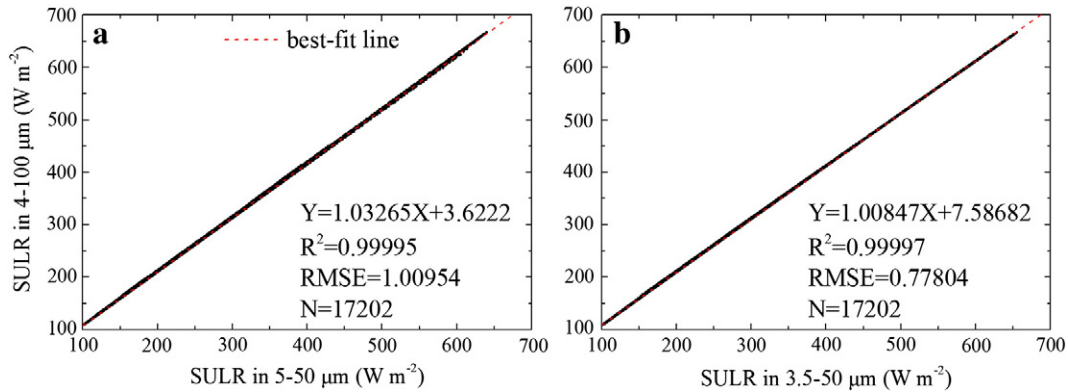


Fig. 4. Histograms of SULR difference in the spectral ranges a) between 4–100 μm and 3.5–50 μm and b) between 4–100 μm and 5–50 μm.



**Fig. 5.** The linear fit for SULRs between spectral ranges of a) 4–100  $\mu\text{m}$  and 5–50  $\mu\text{m}$  and b) 4–100  $\mu\text{m}$  and 3.5–50  $\mu\text{m}$ . The red dash line is the best fit line.

transmission range is approximately 3.5 to 50  $\mu\text{m}$  (Fairall, Persson, Bradley, Payne, & Anderson, 1998).

There are different spectral ranges of radiometers and the estimated SULR (4–100  $\mu\text{m}$ ). The MODTRAN simulations were performed to correct this spectral mismatch before the measurements were used for validation. Six model atmospheres were used, including Tropical Atmosphere (15° North Latitude), Mid-Latitude Summer (45° North Latitude), Mid-Latitude Winter (45° North Latitude), Sub-Arctic Summer (60° North Latitude), Sub-Arctic Winter (60° North Latitude) and 1976 US Standard Atmosphere. The surface properties were described by 47 spectral emissivity data from the MODTRAN in-built emissivity database. The surface temperature ranged from 210 to 330 K with the increment of 2 K. Thus there were 17,202 ( $6 \times 47 \times 61$ ) scene cases in total. The concentration of carbon dioxide was 390 ppm and the rural aerosol model was used to indicate the type of extinction and meteorological range of the boundary layer. The surface height was 0.0 km and the sensor was located at 100 km altitude with the nadir view. The simulation results presented in Fig. 4 suggest that the discrepancies are significant about 7 to 13  $\text{W m}^{-2}$  for the spectral ranges between 4–100  $\mu\text{m}$  and 3.5–50  $\mu\text{m}$  with a peak of 11.5  $\text{W m}^{-2}$ , and about 7 to 27  $\text{W m}^{-2}$  for the spectral ranges between 4–100  $\mu\text{m}$  and 5–50  $\mu\text{m}$  with a peak of 10  $\text{W m}^{-2}$ . Consequently wider spectral range causes less variance of this discrepancy.

The linear conversions were established based on this simulation dataset (Fig. 5). For the conversion from SULR in the spectral range of 5–50  $\mu\text{m}$  to SULR in 4–100  $\mu\text{m}$ , RMSE is 1.00954  $\text{W m}^{-2}$  and R-square ( $R^2$ ) is 0.99995. While for the conversion from SULR in the spectral range of 3.5–50  $\mu\text{m}$  to SULR in 4–100  $\mu\text{m}$ , RMSE is 0.77804  $\text{W m}^{-2}$  and  $R^2$  is 0.99997, which indicate a higher regression precision due to a wider spectral range and thus similar radiant energy. Finally, we adjusted the in situ measured longwave radiation data by these two linear functions in order to match the spectral range used in our model.

### 3. Methods

#### 3.1. Radiative transfer simulation

The hybrid method requires a simulation database to train the statistical model, for instance the ANN model in this paper. MODTRAN was employed to build a comprehensive simulation database to represent the true conditions of the Tibetan Plateau as far as possible with a variety of atmosphere and surface conditions. MODTRAN is a widely used sophisticated radiative transfer model in fields of the atmospheric science and remote sensing, which can simulate the complicated interactions of radiant energy within the atmosphere and at the surface (Berk et al., 1999; Berk et al., 2006). The input parameters consist of atmospheric profiles, surface temperature and emissivity, sensor zenith angle, spectral response functions and other required parameters.

The representative atmospheric profiles within the Tibetan Plateau were extracted from MOD07/MYD07 data, which can depict the atmospheric conditions with vertical changes of the air temperature and humidity. Five criteria were applied to screen high-quality profiles according to the analysis and comparison of those data: 1) the surface temperature should be greater than 220 K; 2) the difference of air temperature or dew point temperature between two adjacent layers should be less than or equal to 20 K; 3) the altitude of the lowest layer should not be higher than the surface elevation; 4) the air temperature should be greater than the dew point temperature; 5) the relative humidity should be less than 90% for clear-sky profiles (Tang & Li, 2008).

Although the above criteria were applied, most selected profiles were very similar in terms of vertical variation and shapes. These redundant profiles could dramatically increase computation time and lead to analogous simulation results. In order to alleviate the similarity and reduce the total number of profiles, meanwhile enhance the representation of atmospheric profiles, a topological method for refining vertical profiles of atmospheric temperature and dew point temperature was adopted. This approach follows some assemble pattern and screens profiles with air temperature differences and dew point temperature differences greater than certain threshold values (Sharma & Ali, 2013; Wang & Liang, 2010; Wang et al., 2012). Finally 1608 MODIS profiles were chosen.

Other parameters were set as follows. The surface condition is another important aspect for surface upward longwave radiative flux. It can be expressed by the surface temperature and spectral emissivity. The surface skin temperature data were extracted from MOD07/MYD07 data for each profile and modified by five delta values as  $\pm 10$ ,  $\pm 5$  and 0 K. Spectral emissivity data were selected as described in Section 2.2. The satellite zenith angles were from 0 to 70° with 10° interval. Because the view zenith angles approach 65° and 70° at the end of a scan line at the Earth's surface of the MODIS and VIIRS instruments, respectively. These are corresponding to  $\pm 55^\circ$  scanning angles of MODIS (Barnes et al., 1998), and  $\pm 56.28^\circ$  angles in the cross-track direction of VIIRS (Cao et al., 2013). The spectral response functions of MODIS and

**Table 4**  
The input and output settings for the MODTRAN simulation.

|        | Variables   | Unit or range   |
|--------|---|---|
| Input  | Sensor zenith angle (°)<br>Spectral emissivity<br>Surface temperature (K)   | 0, 10, 20, 30, 40, 50, 60, and 70<br>52 spectrum<br>LST from MOD07/MYD07 plus delta values ( $\pm 10, \pm 5$ and 0 K) |
| Output | Atmospheric profile<br>Radiance of MODIS bands 29, 31, 32 and 33, and VIIRS bands M14, M15 and M16<br>Surface upward longwave radiation | 1608<br>$\text{W m}^{-2} \text{sr}^{-1} \mu\text{m}^{-1}$<br>$\text{W m}^{-2}$  |

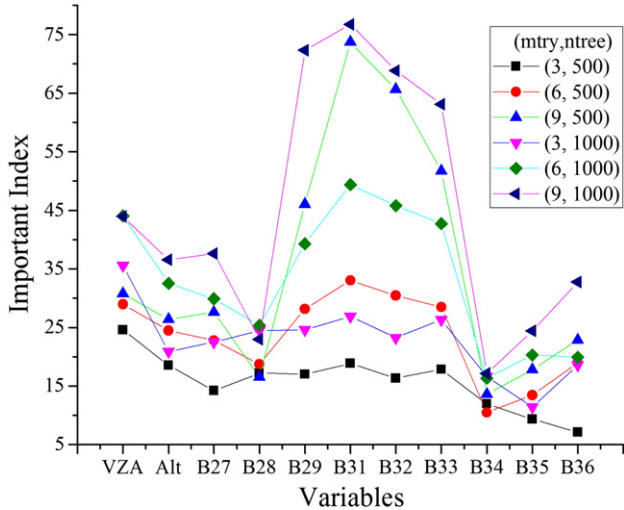


**Fig. 6.** Variable important index using the RF method according to different mtry and ntree values. VZA is the view zenith angle. Alt is the surface elevation. B27 is the TOA radiance of MODIS band 27 and so on.

VIIRS used were shown in Fig. 1. Additionally, other input parameters, such as aerosol type, molecular gases or auxiliary gaseous species, etc. were assigned the values of the specified model atmosphere according to the acquisition time and latitude of each profile. The detailed settings are listed in Table 4.

### 3.2. Variable selection

The selection of variables applied to the ANN model is an important procedure because only variables containing important information to derive SULR can be imported into the ANN model. Meanwhile it is not as many variables as good due to the fact that the uncertainty and deviation errors of input data can undermine the valid information and thus decrease the retrieval accuracy of SULR. Therefore, enough and less input data are the tradeoff.

The Random Forest (RF) method was firstly used to investigate the significance of different parameters. The RF method is a fast and highly accurate ensemble learning method for classification and regression with a large number of input variables (Breiman, 2001). It constructs a collection of decision trees by the bootstrap sampling method and variables at each node are randomly selected from all input variables. After the training procedure, the random forests are built and can be used for classification or regression. It can also be used in estimating the importance of variables and detecting variable interactions in the

**Table 5**  
The designed cases of variable combinations.

| Case   | Combinations        |
|--------|---------------------|
| Case 1 | Bands 29, 31 and 32 |
| Case 2 | Case 1 + B33        |
| Case 3 | Case 2 + VZA        |
| Case 4 | Case 2 + Alt        |
| Case 5 | Case 2 + VZA + Alt  |

regression analysis (Diaz-Uriarte & Alvarez de Andres, 2006; Strobl, Boulesteix, Zeileis, & Hothorn, 2007). The importance index derived from the RF method is a good indicator whether a variable is more important for the output parameter than other variables in the input dataset or not. The higher the importance index is, the more important the variable is. RF method was employed on variables including view zenith angle (VZA), surface altitude (Alt) and MODIS TOA radiances in the MODTRAN simulation dataset. The number of input variables randomly chosen at each node (mtry) and the number of trees in the forest (ntree) are two key parameters in the RF method. And mtry was set to 3, 6, and 9; and ntree was set to 500 and 1000. The results (Fig. 6) indicate that radiances of bands 27, 29, 31, 32, 33, and 36, VZA and Alt are more sensitive than the other variables in different combinations of mtry and ntree values.

Further simulation of MODIS TOA radiances was carried on so as to check the sensitivity for various surface emissivities and temperatures. The 52 spectral emissivity data were used in the simulation with the 1976 US Standard Atmosphere and the surface temperature of 300 K. MODIS bands 29, 31, 32, 33 and 34 are sensitive for different emissivities but radiances of bands 27, 28, 35 and 36 are almost unchanged from Fig. 7a. The surface temperatures were set from 260 to 330 K with an increment of 10 K for exhibiting the influence on TOA radiances under the 1976 US Standard Atmosphere and the emissivity of 0.8. Fig. 7b shows that bands 29, 31, 32 and 33 are more sensitive for LST variance. The atmospheric window channels are a good choice for estimating SULR (Wang & Liang, 2010).

The sensitive bands were imported into the ANN model to test the regression accuracy under different variable combinations as listed in Table 5. Case 1 with MODIS bands 29, 31 and 32 was mainly referred to the work of Wang and Liang (2009). Cases 3 to 5 were based on the result of case 2. Because when MODIS band 33 was added as the input parameters of the ANN model, RMSEs had a relatively high decline from about 13.5 to 11.5 W m<sup>-2</sup> for the best situation in Fig. 8. When the surface altitude was included, the variability of RMSE became high. Nevertheless, VZA can enhance the stability of RMSE due to less variance in case 3.

In conclusion, TOA radiances of MODIS channels 29, 31, 32, and 33 and VZA are sensitive to retrieving SULR and were selected as the

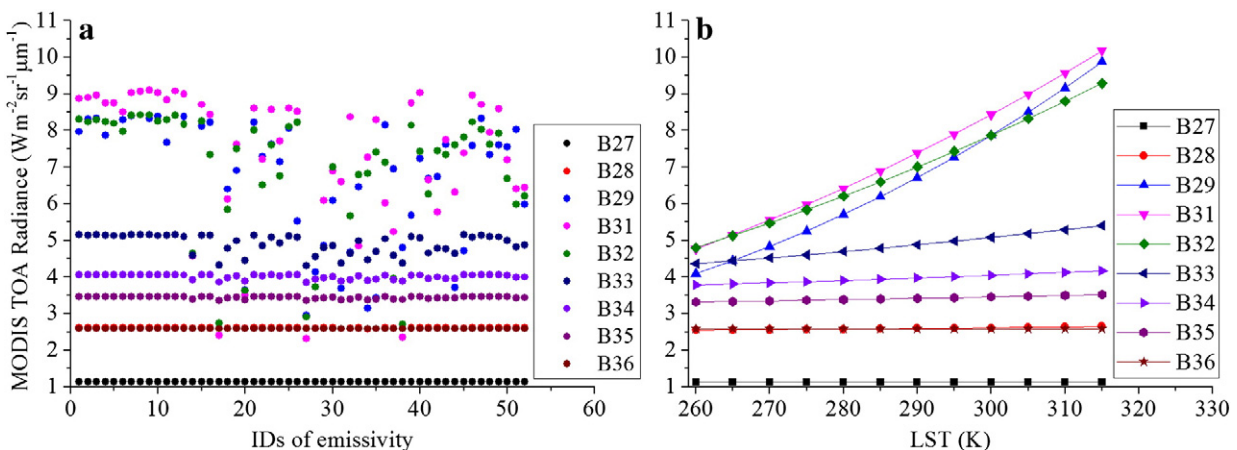


**Fig. 7.** MODIS TOA radiances simulated by MODTRAN for a) different spectral emissivity data and b) different land surface temperatures.

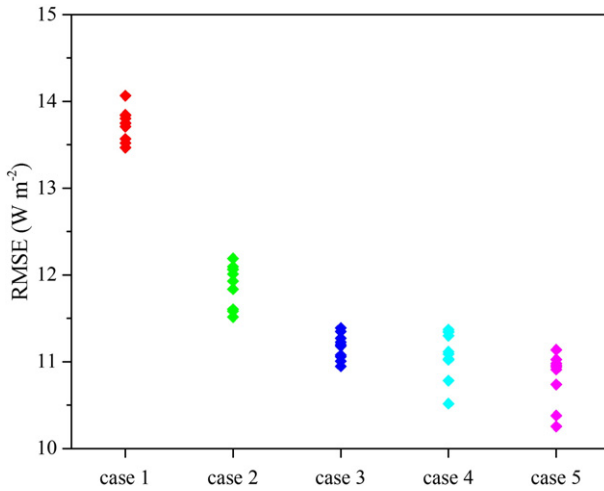


Fig. 8. RMSEs of the ANN model for five cases.

input parameters in the ANN model. Accordingly, VIIRS channels M14, M15, and M16 and VZA were the main inputs for estimating VIIRS SULR, but no similar channel as MODIS band 33 could be added. They are within the atmospheric window and thus sensitive to the surface upwelling longwave radiative flux. The absorption differences of the water vapor among the bands make the potential to correct the effects of water vapor on the longwave radiation. And VZA can take the nonlinearity of TOA radiances under various sensor view directions into account (Wang & Liang, 2010; Wang et al., 2009). When VZA is included as input parameters in the ANN model, it can derive the reasonable result or even better than the single VZA model based on a MODTRAN simulated test (not shown). This reduces the uncertainty that is caused by the linear interpolation of SULRs in two presupposed VZAs when the input VZA doesn't belong to theirs, especially when the designed span of VZAs is large such as  $10^\circ$  or more.

### 3.3. SULR retrieved by the ANN model

The ANN model is a statistical model in which “neurons” are connected together to form a network which resemble a biological neural network. It consists of sets of adaptive weights, biases, i.e. which are tuned by the learning algorithm, and is capable of performing nonlinear regression and pattern recognition (Kim, 2004). ANN provides a computationally efficient and robust way to determine an empirical, nonlinear relationship between multi-inputs and one or more outputs (Krasnopolsky, Fox-Rabinovitz, & Chalikov, 2005).

A single hidden layer feed-forward neural network was used here to model SULR. In general, the number of neurons in the hidden layer is a sensitive factor. Too many neurons usually cause overfitting of the ANN model, while less neurons frequently lead to underfitting and low correlation. We iteratively conducted the ANN simulations by only changing the number of neurons in the hidden layer from 6 to 15 and finally decided the number with the least model fitting error. In this study, 11 and 9 neurons in the hidden layer were selected for the MODIS-based and VIIRS-based model. The input and output of the ANN simulation are displayed in Table 6. MODIS band 29 is the water vapor channel; bands 31 and 32 are related to the skin temperature, and have a strong

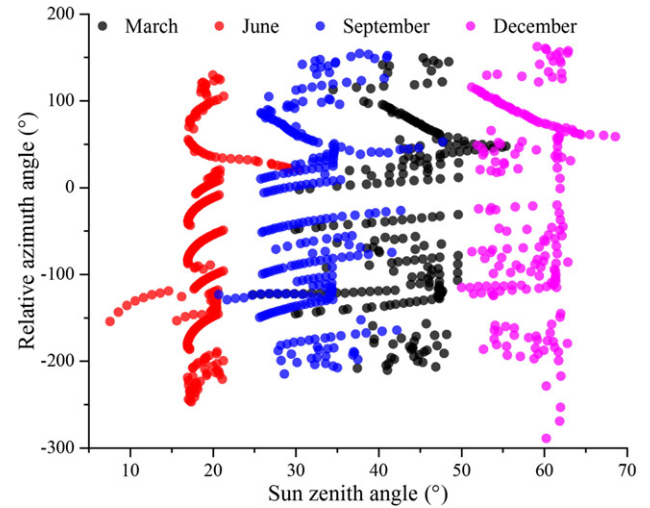


Fig. 9. Scatterplot of the sun zenith angle and relative azimuth angle from MOD07 data within the Tibetan Plateau in 2012.

linear relationship with SULR (Barnes et al., 1998; Tang & Li, 2008); Band 33 is relevant to the near surface temperature. The radiances measured in VIIRS channels M14, M15 and M16 were inputs in the VIIRS-based ANN retrieval model. Additionally, sensor view zenith angle was used to calibrate the nonlinear effect in the SULR retrieval.

## 4. Sensitivity analyses

### 4.1. Impact of solar illumination on the SULR simulation

The MODTRAN simulation was performed based on similar conditions in Section 2.3, but the spectral range was set to 4–100  $\mu\text{m}$ . The full radiation mode and thermal mode were used to evaluate the impact of the solar illumination. When full radiation mode was used, the Mie-generated internal database of aerosol phase functions was selected and day of year was set to 93. In order to choose the typical sun angles, the solar and sensor zenith and azimuth angles were extracted from MOD07 data within the Tibetan Plateau in March, June, September and December of 2012. The relative azimuth angle was calculated by the sun azimuth angle minus the sensor azimuth angle. We chose four representative angle combinations  $(20^\circ, 0^\circ)$ ,  $(30^\circ, 100^\circ)$ ,  $(40^\circ, -100^\circ)$ ,

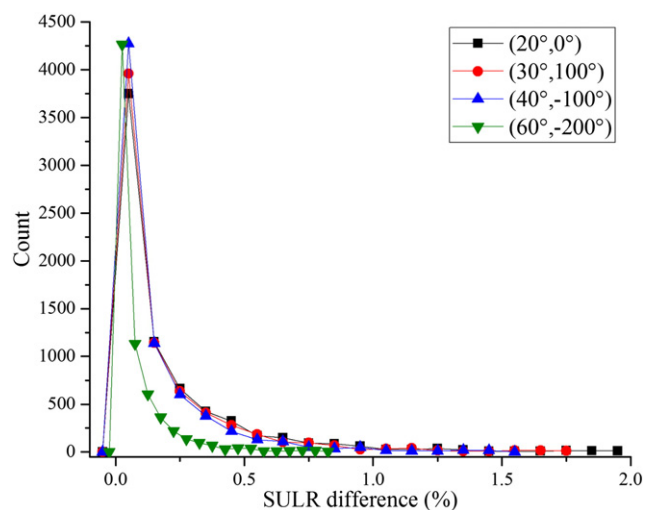
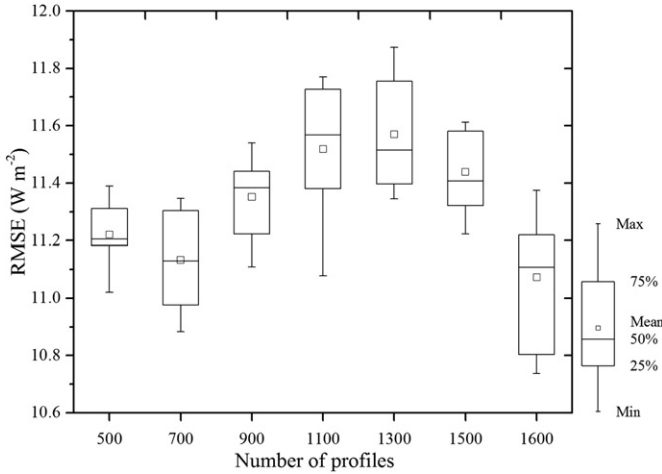


Fig. 10. Histograms of SULR differences in percent between the full radiation mode and thermal mode for four cases with different combinations of the sun zenith angle and relative azimuth angle.

Table 6

Variables used in the ANN simulation.

|        | Variables   | Unit  |
|--------|---|---|
| Input  | Radiances of MODIS bands 29, 31, 32 and 33, or VIIRS bands M14, M15 and M16 | $\text{W m}^{-2} \text{sr}^{-1} \mu\text{m}^{-1}$ |
| Output | Sensor view zenith angle<br>Surface upward longwave radiation               | Radian<br>$\text{W m}^{-2}$                       |



**Fig. 11.** Sensitivity of the quantity of profiles on the ANN model.

and  $(60^\circ, -200^\circ)$  in the sun zenith angle and relative azimuth angle based on the relationship between them in Fig. 9.

The histograms of SULR differences between the full radiation mode and thermal mode for four representative cases were shown in Fig. 10. The differences are mainly focused on about 0.1% although the maximum can reach to circa 2%. With the increase of sun zenith angles, the impact of sun illumination becomes smaller, especially for the maximum of differences. This is because the larger sun zenith angles can cause more atmospheric absorptions on the solar radiation, leading to less energy into the land surface. Because of the limited impact on the retrieval of SULR, the thermal model was chosen in the MODTRAN simulation.

#### 4.2. Impact of the quantity of profiles on the SULR retrieval

The sensitivity of the quantity of profiles on the SULR retrieval was analyzed. The numbers of profile were set to 500, 700, 900, 1100, 1300, 1500 and 1600. In each case, samples with specific quantity were extracted randomly from the dataset of 1608 profiles. The ANN model was carried out 10 times to get the histogram of RMSEs in each case (Fig. 11). The mean RMSE of each case ranges from about  $11.1$  to  $11.5 \text{ W m}^{-2}$ . The maximal and minimal RMSEs are about  $11.9 \text{ W m}^{-2}$  and  $10.7 \text{ W m}^{-2}$ . These indicate that profile quantity cannot significantly affect the regression accuracy of the ANN model. The key factor is the

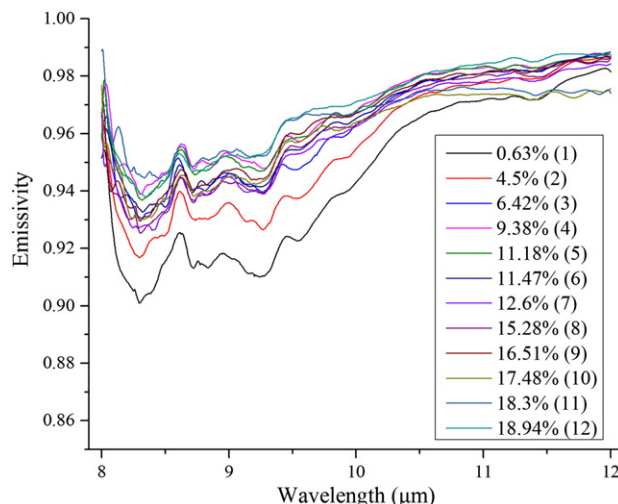


**Fig. 12.** Soil emissivities with different soil moistures. The percent is the soil water content and the number in the bracket is the serial number used in Fig. 13.

**Table 7**  
The major variables and ranges for the MODTRAN simulation.

| Variables                      | Ranges                         |
|--------------------------------|--------------------------------|
| Atmosphere mode                | 1–6                            |
| Surface temperature (K)        | 260 to 320 with increment of 5 |
| Altitude (km)                  | 0.0, 1.0, 3.0 and 5.0          |
| View zenith angle ( $^\circ$ ) | 0, 20, 40 and 60               |

representativeness of the atmospheric profile itself, which will be discussed in Section 5.1. Meanwhile, SULR is less sensitive to atmospheric conditions, but dominated by the surface properties. There are at most 16 layers in the atmospheric profiles from MOD/MYD07 data, therefore coarser vertical resolution causes less variation compared with the fine-resolution radiosonde data. So more profiles may not increase more information about atmospheric conditions.

#### 4.3. Impact of the emissivity dataset on the retrieval method

It is known that surface emissivity depends on soil water content and can induce model biases in the estimation of LST and surface radiative fluxes (Hulley, Hook, & Baldridge, 2010; Mira et al., 2010; Rubio, Caselles, & Badenas, 1997; Xiao et al., 2003). The influence of soil moisture can cause land surface emissivity increase from 1.7% to 16% and brings in systematic biases to the LST about 0.1 to 2 K (Mira, Valor, Boluda, Caselles, & Coll, 2007).

In order to determine the impact of emissivities with different soil moistures on the ANN model for the SULR retrieval, a simulation experiment was performed. The emissivity data with different soil water contents used to describe the surface characteristics in MODTRAN are shown in Fig. 12. The soil water contents are from 0.63% to 18.94% and higher soil moisture generally leads to higher soil emissivity. The settings of major variables in the MODTRAN simulation are listed in Table 7. The simulated results were feed into the ANN model to derive SULR. The estimated SULR was compared with MODTRAN simulated values, and the results can be seen in Fig. 13. The differences for emissivities with different soil water contents are all near zero, although the magnitude of extrema can reach to near  $50 \text{ W m}^{-2}$  and  $-20 \text{ W m}^{-2}$ . It suggests that the variability of land surface emissivity due to soil moisture cannot influence the retrieval accuracy of the ANN-based SULR model remarkably. Therefore, the differences between the ANN retrieved and MODTRAN calculated SULR are insensitive to soil water contents.

The emissivity dataset used in the MODTRAN simulation consists of 52 spectral emissivity data. The representativeness of the emissivity

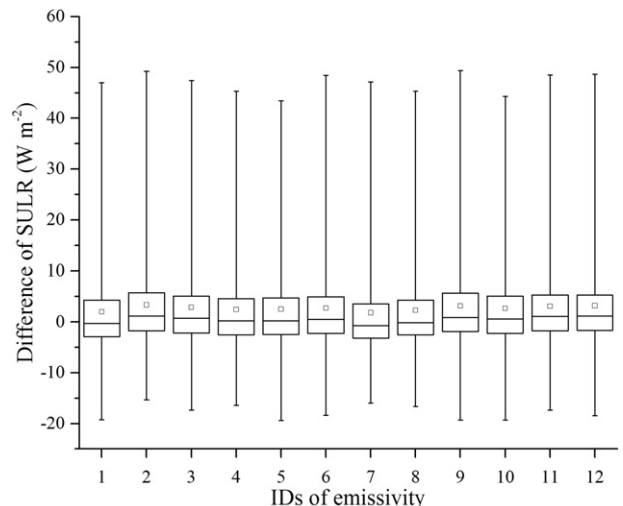


**Fig. 13.** Boxplots of differences between ANN model's SULR and that from MODTRAN for 12 spectral emissivities with different soil moistures.

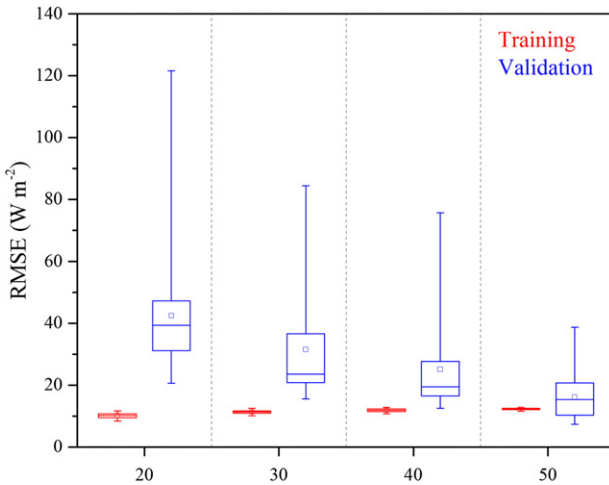


**Fig. 14.** Boxplots of training (red) and validation (blue) RMSEs in the ANN model with 10 to 50 spectral emissivities in the training stage based on the cross-validation method. The results using 10 spectral emissivities are not shown due to the large validation RMSEs beyond  $500 \text{ W m}^{-2}$ .

dataset was carried on based on the cross-validation method. The spectral emissivities were randomly selected from the emissivity dataset by the numbers of 10, 20, 30, 40 and 50 as the training data, and the remaining emissivities were used in the validation stage. Each case was repeated 30 times to derive the statistical results. In Fig. 14, the red boxplots are training RMSEs and the blue ones are validation RMSEs. The results using 10 spectral emissivities are not shown due to the large validation RMSEs beyond  $500 \text{ W m}^{-2}$ . It is shown that the training RMSEs are relatively stable hovering around  $10$  to  $13 \text{ W m}^{-2}$ , but the validation RMSEs vary dramatically. Less emissivity data can lead to

larger uncertainty in retrieved SULR due to inadequate representativeness. When adding more spectral emissivities in the training dataset, the mean validation RMSEs become smaller from  $42.5$  to  $16.2 \text{ W m}^{-2}$ , making the ANN model more robust. Moreover, the emissivity dataset was selected based on the principle of maximum variance among three emissivity libraries. Each spectral emissivity is very different from each other, therefore any spectral emissivity cannot be well represented by others, which is a reason for the high discrepancy between the training and validation RMSEs. Generally the ANN model can adapt to different emissivities under all kinds of atmospheric and surface conditions, and the emissivity dataset used can basically satisfy the requirement.

## 5. Results and discussion

### 5.1. Statistical characteristic of the simulation database

The generalization ability of the ANN model is actually based on the interpolation rather than extrapolation. Therefore, it is required that the input and output for training the ANN model should contain all possible situations. The upper and lower limits should be wide enough, meanwhile the uniform distribution of values of samples within limits is also expected. The quality of atmospheric profile database is critical to depict the real atmospheric conditions in the Tibetan Plateau. The detailed evaluation of MOD07/MYD07 data can refer to the work by Seemann et al. (2003). In order to further verify the validity, we investigate the distribution characteristics of the profile database with five variables (Fig. 15) and the simulation results of SULR in Fig. 17.

Three key parameters are total column perceptible water vapor (TCPWV), surface elevation and skin temperature. First, TCPWV is the depth of water in a column of the atmosphere if all the water is concentrated together in centimeter. It is the quantity of total atmospheric water vapor content which is the most abundant greenhouse gas that emits and absorbs the atmospheric longwave flux (Naud, Chen,

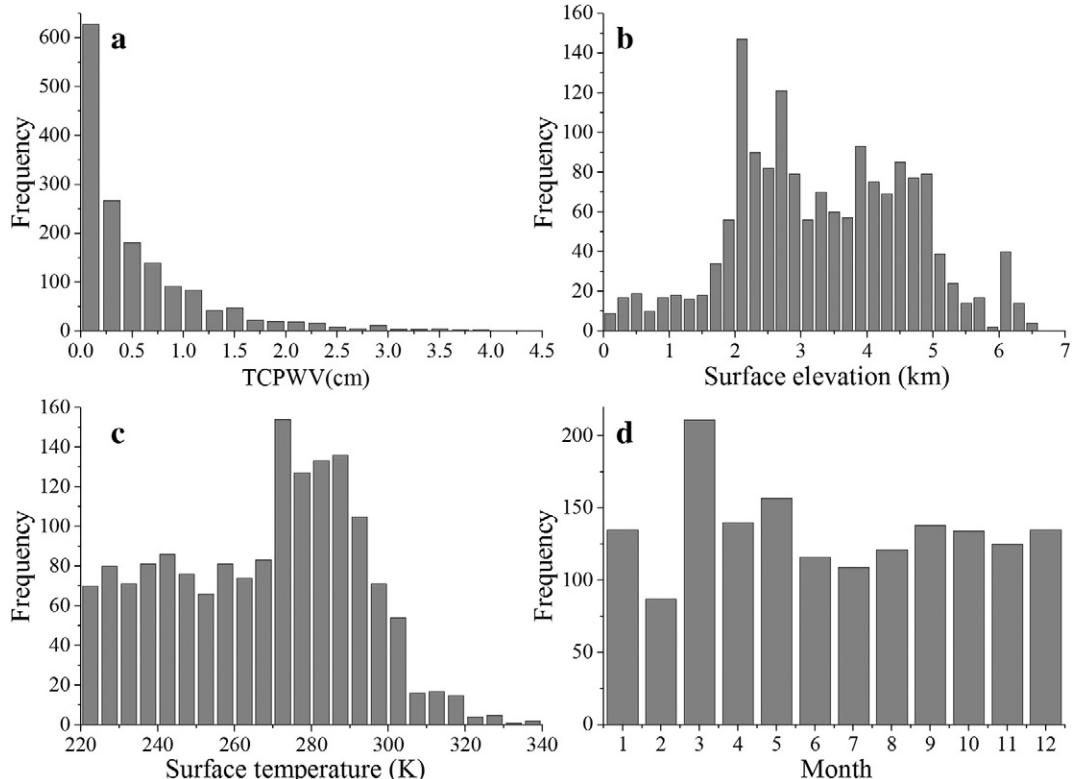


**Fig. 15.** The statistical histograms of the atmospheric profile database from MOD07/MYD07 data.

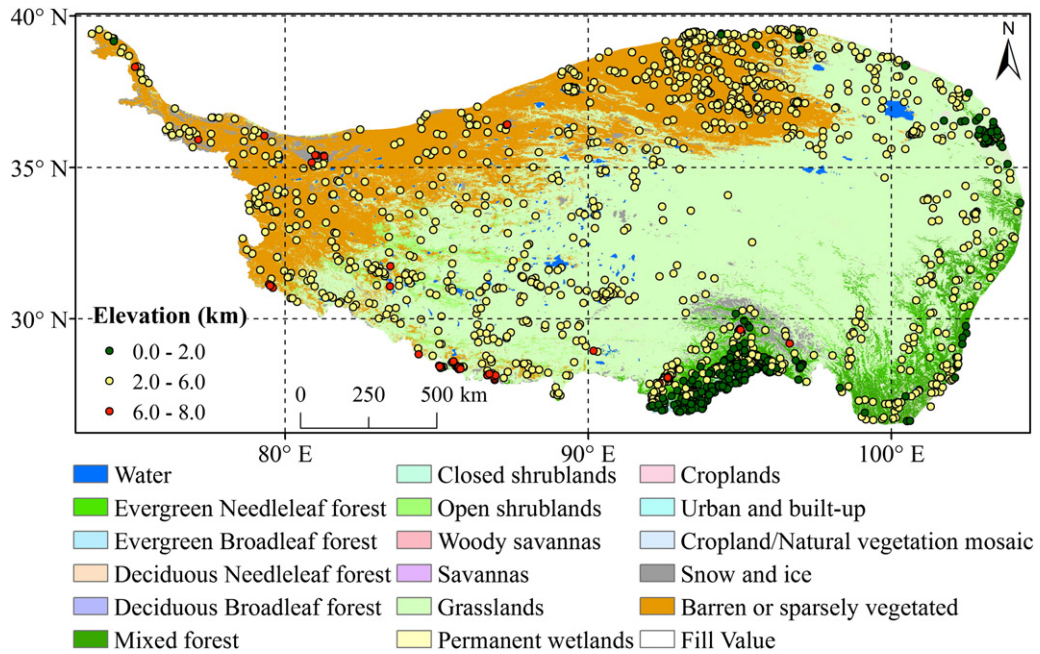


**Fig. 16.** The spatial distribution of MOD/MYD07 profiles (the circles) in the atmospheric profile database. The surface types were from MCD12Q1 data in 2012 based on the IGBP scheme in the Tibetan Plateau.

Rangwala, & Miller, 2013; Stephens et al., 2012). TCPWV ranges from 0.01 to 4.489 cm with a mean of 0.532 cm (Fig. 15a) and exhibits the trend of exponential decay with most aggregated in 0 to 1.5 cm that is consistent with the result of Zhang, Wang, Zhai, Gu, and He (2013). This indicates the relative low-humidity atmospheric condition in the Tibetan Plateau. Second, the elevation range of this database is from 0 to 6.53 km (Fig. 15b), which covers the main altitude distribution in the Tibetan Plateau and the valley areas with elevation less than 2 km. Third, surface skin temperatures were from 220 to 340 K (Fig. 15c). This range can include all possible temperatures, thus it is enough for the simulation and modeling.

The features of spatiotemporal distribution also satisfy the requirement. The result shows a good uniformity of month distribution (except February with 87 profiles and March with 211 profiles) that can guarantee the inclusion of seasonal effect on the SULR retrieval model (Fig. 15d). The spatial distribution of profiles is presented in Fig. 16. The background's surface types were from MCD12Q1 data in 2012 based on the IGBP scheme in the Tibetan Plateau. There are 7 dominating surface types: Grasslands, Barren or sparsely vegetated, Mixed forest, Open shrublands, Snow and ice, Evergreen Needleleaf forest and Water. Most surface types were covered by some profiles. Few profiles are distributed in the center of the Tibetan Plateau. This is probably because this region has homogeneous and stable atmospheric environment, hence a handful of profiles can stand for the atmospheric conditions. Meanwhile more profiles are located near the margins of the Tibetan Plateau, such as the junctures of Himalaya Mountains, Taklimakan Desert and Qaidam Basin. These areas have the larger elevation variation that causes dramatically changes of air temperature and humidity. The profiles (green circles in Fig. 16) with lowest altitude less than 2 km are concentrated in the south and east where the topography and land cover are diverse and synoptic environment is changeable, thus lead to greater variability of atmosphere profiles.

As the retrieval target, SULR's distribution demonstrates the rationality of the simulation database. The ranges of SULR data for MODIS and VIIRS are almost the same from about 30 to 700 W m<sup>-2</sup> with a mean of 259.355 W m<sup>-2</sup>. These correspond to the equivalent brightness temperatures as a blackbody from 152 to 333 K according to the Stefan-Boltzmann law, which covers all possible surface temperature.

Furthermore, they mainly concentrate from about 170 to 450 W m<sup>-2</sup>, a major variation in the Tibetan Plateau (Shi & Liang, 2013; Yang et al., 2006).

### 5.2. ANN training results

Three indices were chosen to characterize the accuracy of the SULR retrieval: the coefficient of determination ( $R^2$ ), mean bias error (MBE) and root-mean-square error, which are defined as follows:

$$R^2 = \frac{\left( \sum_{i=1}^n (E_{i,true} - \bar{E}_{true}) (E_{i,derived} - \bar{E}_{derived}) \right)^2}{\sum_{i=1}^n (E_{i,true} - \bar{E}_{true})^2 \cdot \sum_{i=1}^n (E_{i,derived} - \bar{E}_{derived})^2}, \quad (2)$$

$$MBE = \frac{1}{N} \sum_{i=1}^N (E_{i,derived} - E_{i,true}), \quad (3)$$

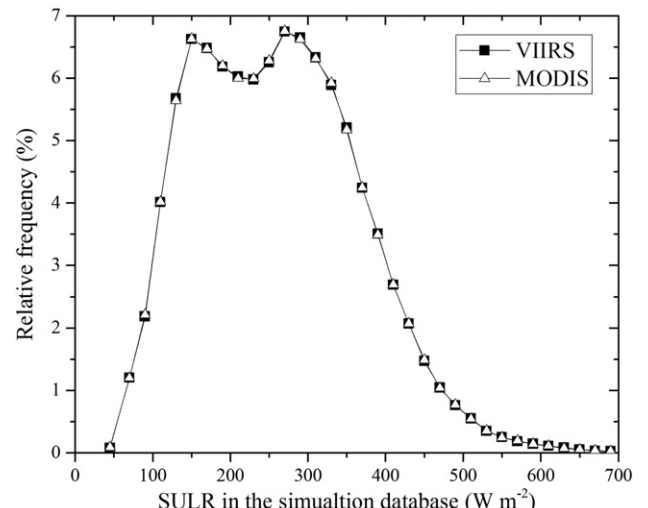


**Fig. 17.** The statistical histograms of SULR in the simulation database.

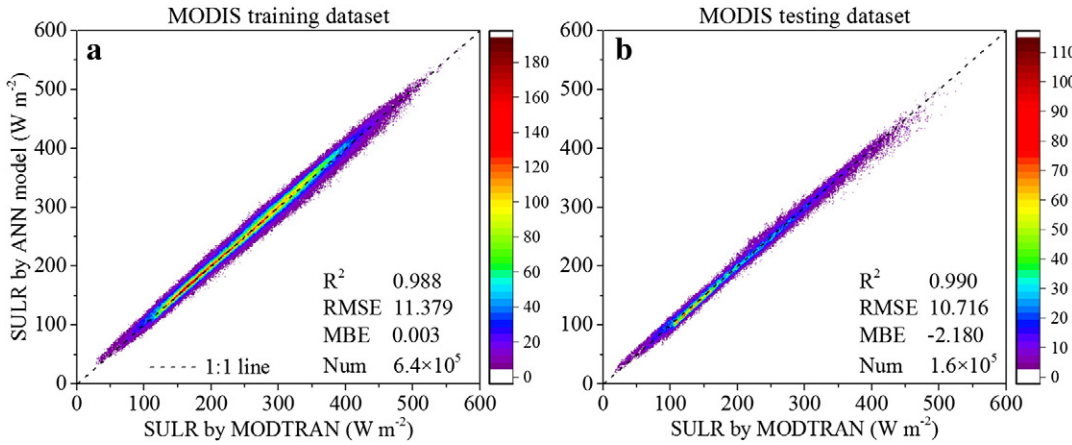


**Fig. 18.** ANN simulation results for MODIS a) training and b) testing dataset. The color scale is given as the point quantity.

$$\text{RMSE} = \sqrt{\frac{1}{N} \sum_{i=1}^N (E_{i,\text{derived}} - E_{i,\text{true}})^2}, \quad (4)$$

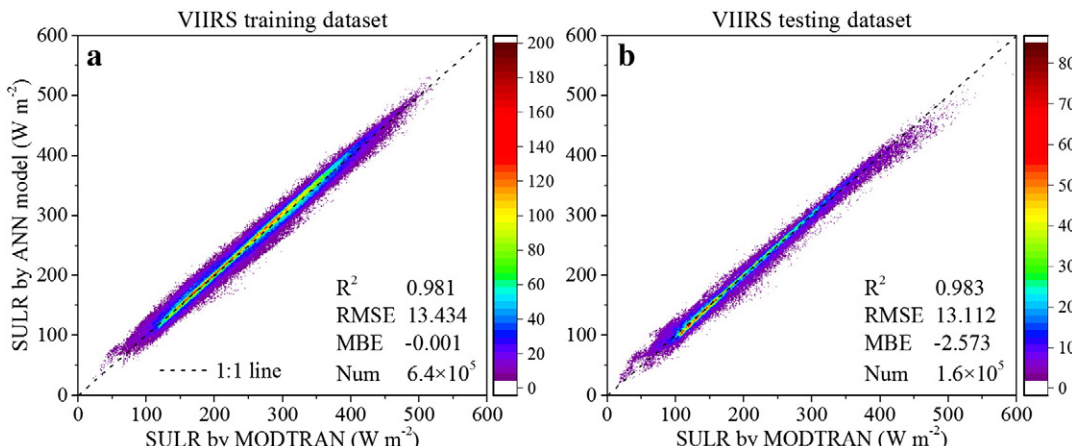
where  $N$  is the sum of samples,  $E_{i,\text{derived}}$  is the model derived SULR,  $E_{i,\text{true}}$  is the true SULR which is either the value simulated by MODTRAN or ground measured value,  $\bar{E}_{\text{true}}$  is the mean of all  $E_{i,\text{true}}$ , and  $\bar{E}_{\text{derived}}$  is the mean of all  $E_{i,\text{derived}}$ .

Fig. 18 is the ANN training results for MODIS data. The number of the legend is the point quantity. The range of SULR is from 30 to 600  $\text{W m}^{-2}$ . The training and testing dataset were divided stochastically by the rate of 80% and 20%. Most of the points follow one-to-one dash line for both MODIS training and testing dataset. The agreement between the ANN model fitting and the radiative transfer model computations is very good. For the training dataset with about 0.64 million samples,  $R^2$  is 0.988, RMSE is  $11.379 \text{ W m}^{-2}$ , and MBE is  $0.003 \text{ W m}^{-2}$ . For the testing dataset with about 0.16 million samples,  $R^2$  is 0.990, RMSE is  $10.716 \text{ W m}^{-2}$ , and MBE is  $-2.180 \text{ W m}^{-2}$ . The similar results are shown in Fig. 19 for VIIRS data, but the regression results are not as good as MODIS'. The  $R^2$ , RMSE and MBE are 0.981,  $13.434 \text{ W m}^{-2}$  and  $-0.001 \text{ W m}^{-2}$  respectively for the training dataset, and 0.983,  $13.112 \text{ W m}^{-2}$  and  $-2.573 \text{ W m}^{-2}$  for the testing dataset. One possible reason is the lack of similar band in VIIRS instrument like MODIS band 33, whereas band 33 can offer some complementary information that enhances the retrieval accuracy.

### 5.3. Validation of the MODIS SULR

The ground measured data were used to further validate the proposed method. MOD021KM data were screened using MOD35 cloud mask data in 2007 and 2008. The pixel of one station was considered to be clear when the  $3 \times 3$  neighborhood were all clear. When at least two stations were under the clear-sky condition in one MOD021KM image, it was deemed to be valid and then was processed to retrieve SULR imagery. As a matter of fact, the Tibetan Plateau is always covered by clouds during most time of a year when Terra or Aqua satellite overpasses, especially in the eastern part where Station D105, Amdo, NPAM, BJ and Namco are sited. In order to fully verify the ANN model, we checked all MOD021KM granule data in each month during 2007 and 2008. The selected data were preprocessed and put into the ANN model to derive SULR data. According to the geographic position of each ground station, the mean SULR value of pixels in  $3 \times 3$  neighborhood was recorded as the ANN retrieved SULR. About 2140 validation samples were finally collected.

The retrieval results were compared with ground measured SULR data (Fig. 20). The results show that the estimation biases vary among different ground stations.  $R^2$  ranges from 0.941 to 0.842, RMSE ranges from  $21.505$  to  $31.649 \text{ W m}^{-2}$ , and MBE is between  $-5.491$  and  $21.746 \text{ W m}^{-2}$ . When we put all data together,  $R^2$  is 0.886, RMSE is  $26.985 \text{ W m}^{-2}$  and MBE is  $10.812 \text{ W m}^{-2}$  as a whole. The best evaluation result can be found in Station D105 with the minimal



**Fig. 19.** ANN simulation results for VIIRS a) training and b) testing dataset. The color scale is given as the point quantity.

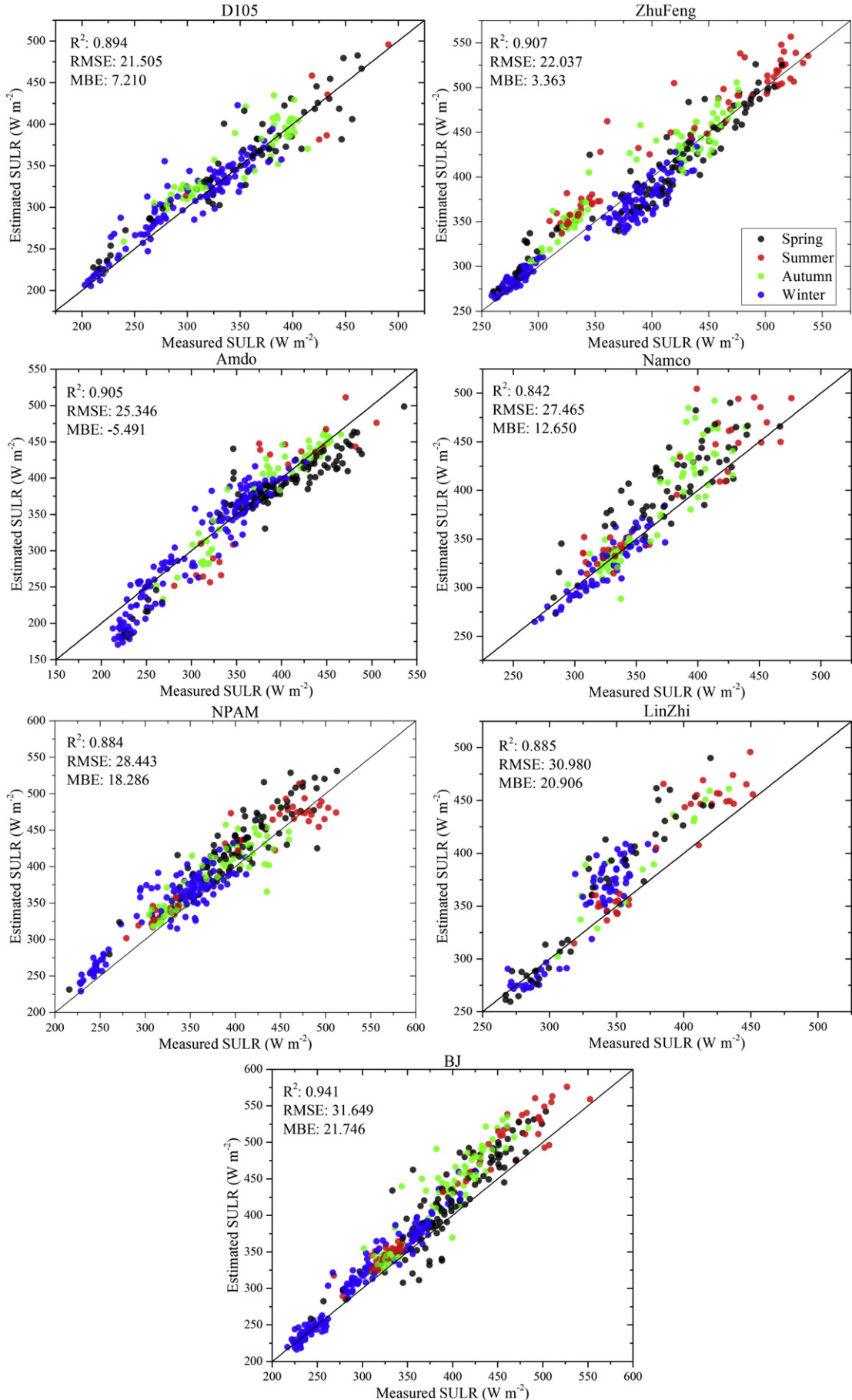


Fig. 20. Scatterplots of MODIS SULR versus ground measurements of 7 stations. The black line is the 1:1 line.

RMSE of  $21.505 \text{ W m}^{-2}$ , but the worst result is in Station BJ due to the obvious overestimation for larger SULR as is also shown for Station Namco. In general, the MODIS SULR is overestimated compared with in situ measurements except Station Amdo where there is an underestimation for smaller value of SULR. And Station ZhuFeng, D105 and Amdo have relatively small deviation. Station Namco, LinZhi and BJ are less closer to the one-to-one line than the other stations. Ideally, no cloud around the ground sites in a wide range is a better situation. Because the validation requires a match-up between ground measurements and satellite imagery. However, the procedures of geolocation and resampling can cause some biases of positions; furthermore, uncertainties of the cloud identification can bring in cloud contamination on pixels where the station locates.

The topography and heterogeneity of the surface cover can also contribute to the inversion errors. The Tibetan Plateau is a topographically complex region. The effect of topography around the sites is significant (Lipton, 1992; Manners, Vosper, & Roberts, 2012; Oliphant, Spronken-Smith, Sturman, & Owens, 2003), especially in Station LinZhi, so the SULR not considering the terrain can have greater deviation compared with ground measurements. Station Namco is located near Lake Nam, which is the largest salt lake in the Tibet Autonomous Region. The distinct difference of land covers in a 1-km resolution pixel can significantly affect the satellite signal, thus make the large biases between retrieved and measured SULR on the shore. The fact that it is difficult to discriminate the cloud and snow/ice in the lake from MOD35 product can also cause nonnegligible influence.

The seasonal difference of the sample pairs is also presented in Fig. 20. The color of each point is based on its month that is divided into four seasons: spring (2, 3 and 4), summer (5, 6 and 7), autumn (8, 9 and 10) and winter (11, 12 and 1). In winter, the SULR ranged from 200 to  $400 \text{ W m}^{-2}$  with variation as high as  $200 \text{ W m}^{-2}$ . But in Station ZhuFeng on the southern-most Tibetan Plateau it ranged from 250 to  $450 \text{ W m}^{-2}$ . Similar variations were found in other seasons. The changes of solar position in different seasons can influence the surface temperature (Senkova, Rontu, & SavijÄrv, 2007). The atmospheric conditions of four seasons also present a distinct difference that leads to diverse incoming solar radiation (Huang, Liu, & Liang, 2011; Zhang, Rossow, & Stackhouse, 2007) and downward sky thermal radiative flux (Naud et al., 2013). The season can change land properties dramatically, such as the cycle of vegetation, snow or ice cover. All of these factors change SULR and impact the retrieval results.

#### 5.4. Comparison with the Wang's method

A linear SULR model was proposed by Wang et al. (2009) (refer it as Wang2009 method), which used TOA radiances of MODIS thermal window channels 29, 31, 32 to infer SULR:

$$\text{SULR} = a_0 + a_1 L_{31} + a_2 L_{32} + a_3 L_{29}, \quad (5)$$

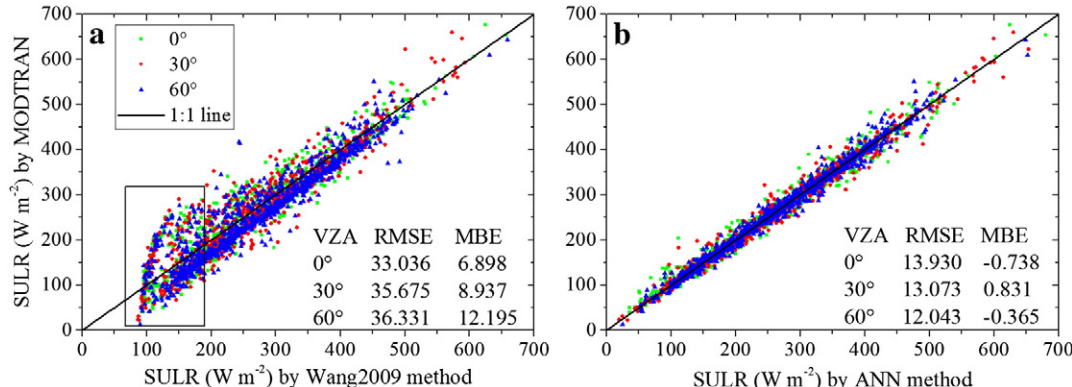


Fig. 21. Comparison between SULR by MODTRAN and that by a) the Wang2009 method or b) the ANN method.

where  $a_0, a_1, a_2$  and  $a_3$  are the regression coefficients. Based on the MODTRAN simulation database, we first extracted 1000 samples randomly at each view zenith angle of  $0^\circ, 30^\circ$  and  $60^\circ$  according to the angle settings in Table 1 of Wang et al. (2009). Next, the multiple linear regression was performed to derive the regression coefficients and the results are presented in Fig. 21a. Lastly, the same dataset was employed by the ANN method (Fig. 21b). For the linear model proposed by Wang et al. (2009), RMSE ranges from  $33.036$  to  $36.331 \text{ W m}^{-2}$ , and MBE ranges from  $6.898$  to  $12.195 \text{ W m}^{-2}$ . The greater discrepancies exist where SULR is within the black box in Fig. 21a. The ANN model can produce better retrieval results with RMSE from  $12.043$  to  $13.930 \text{ W m}^{-2}$  and MBE from  $-0.738$  to  $0.831 \text{ W m}^{-2}$ . Therefore, the nonlinearity between SULR and TOA radiances of MODIS bands can be expressed better by the ANN model.

The SULR data were retrieved based on the method described by Wang et al. (2009), but the regression coefficients were recalculated based on our simulation database although the view zenith angles weren't exactly the same. The retrieved SULR data were evaluated by ground measurements shown in Fig. 22. For the daytime data,  $R^2$  was  $0.704$ , RMSE was  $40.283 \text{ W m}^{-2}$  and MBE was  $21.687 \text{ W m}^{-2}$ ; and  $R^2$ , RMSE and MBE were  $0.838$ ,  $25.310 \text{ W m}^{-2}$  and  $12.949 \text{ W m}^{-2}$  respectively for the night data. The method proposed by this paper can improve the evaluation as presented in Fig. 23 with  $R^2$  of  $0.796$ , RMSE of  $29.653 \text{ W m}^{-2}$  and MBE of  $12.763 \text{ W m}^{-2}$  for the daytime data, and  $R^2$  of  $0.882$ , RMSE of  $19.090 \text{ W m}^{-2}$  and MBE of  $6.115 \text{ W m}^{-2}$  for the night data. These two methods can derive similar scatter pattern from the point of view of different ground stations. For example, MODIS SULR data in Station Amdo were almost underestimated in the night; overestimation could be found for Station BJ. Nevertheless less variance existed for our method. Meanwhile, the retrieval biases were different for the daytime and night data. The night MODIS SULR data are better than the daytime ones for both methods. As a consequence, the ANN-based method can serve as a better solution for retrieving SULR.

#### 5.5. Comparison between MODIS and VIIRS SULR

The publicly available VIIRS images begin from July 2, 2012, but the ground measured radiation data within this period are not available for us, which makes direct estimation impossible at this time. For this reason, evaluation of retrieved SULR from VIIRS data was performed indirectly by comparing it with retrievals from MODIS data. The acquisition time of one MODIS granule image is 07:40 (UTC), January 5, 2014 and that of one VIIRS granule image is from 07:41 to 07:46 (UTC) in the same day. The time lag is less than six minutes. Thus it is assumed that no significant differences of atmospheric conditions and land surface properties exist between these two images.

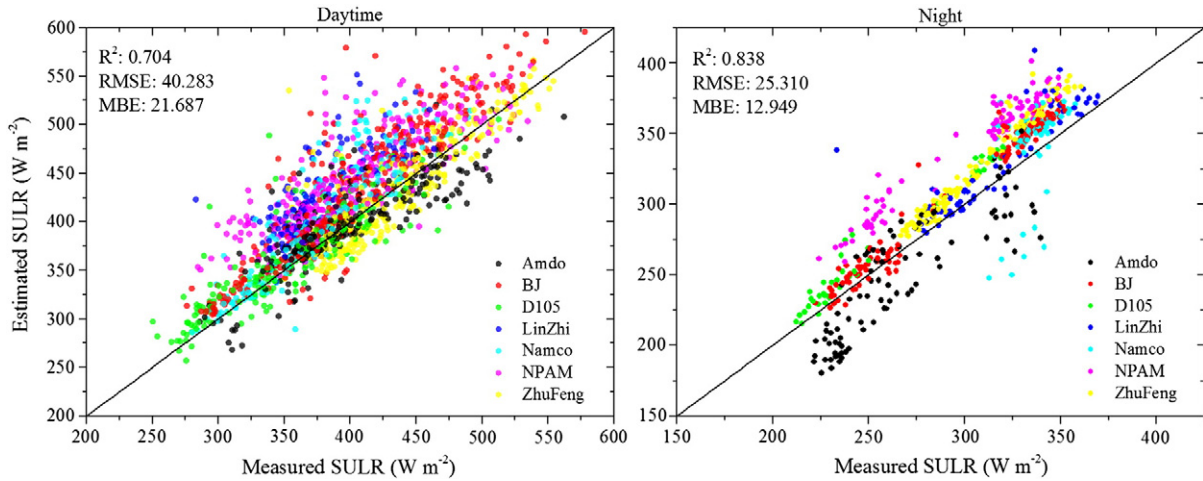


**Fig. 22.** Scatterplots between MODIS SULR and ground measurements using Wang2009 method in the daytime (left) and in the night (right).

The plots of MODIS and VIIRS SULR data over the Tibetan Plateau are shown in Fig. 24. The bold black line is the boundary line of the Tibetan Plateau. The gray lines are administrative boundary lines. And the white areas are covered by the clouds or invalid data. It can be seen from these plots that the spatial distribution patterns of SULR data consistent with each other. The higher values occur in the south of the Tibetan Plateau. At the same time, the lower values are distributed over lake and have closely relationship with the cloud. The cloud shadow can reduce surface temperature and then the upward longwave radiation. The lower upward longwave radiation along the border of the cloud is mainly due to the unidentified cloud pixels or pixels partly covered by clouds. The difference of cloud mask from MODIS and VIIRS products is obvious: more clouds are identified in the northeast corner of the MODIS data. In the local enlarged image plots, VIIRS cloud mask products recognize more clouds within the lake. These biases may be due to the frozen lake confusing the cloud and snow/ice. This is a reason why large discrepancy exists between SULR from MODIS and VIIRS data in Fig. 25.

In order to compare the difference of SULR data from MODIS and VIIRS data, the MODIS SULR were downscaled to 750 m with nearest neighbor resampling method. The SULR data retrieved from both MODIS and VIIRS data were extracted and compared over the whole region excluding the areas covered by clouds or invalid data. The density plot is shown in Fig. 25. Most of the values are concentrated between 300 and 450  $\text{W m}^{-2}$  with  $R^2$  of 0.515, RMSE of 26.021  $\text{W m}^{-2}$  and MBE of 2.869  $\text{W m}^{-2}$ . The VIIRS SULR data have some overestimation

in lower values and underestimation in higher values with respect to MODIS SULR.

As a whole, the retrieval results from MODIS and VIIRS data have a good agreement, although a large discrepancy still exists. The difference may be caused by the following reasons: First, MODIS and VIIRS have different spatial resolutions. The radiance of one pixel in the same geographic position represents different mixed surface temperature and emissivity of heterogeneous land covers unless the surface is homogeneous, isothermal and plane. Furthermore, geolocation for MODIS and VIIRS data is not exactly matched in nature. The slight discrepancy of georeferenced MODIS and VIIRS can be found, especially significant in the edge of lakes, rivers etc. Additionally, the view geometries are not the same for each pixel. Finally, it makes more discrepancy when the effect of topography is superposed on the different view geometry (Lipton & Ward, 1997; Liu, Hiyama, & Yamaguchi, 2006). As a result, high quality in situ measurements are preferred to evaluate the validity of the proposed model using the VIIRS data.

## 6. Conclusions

In this paper, a hybrid method, which combines extensive radiative transfer simulation and the ANN statistical model, is proposed to predict SULR directly from TOA radiances of MODIS and VIIRS thermal infrared window channels as well as satellite view zenith angle over the Tibetan Plateau, a special region, known as the "Third Polar". As a successor of

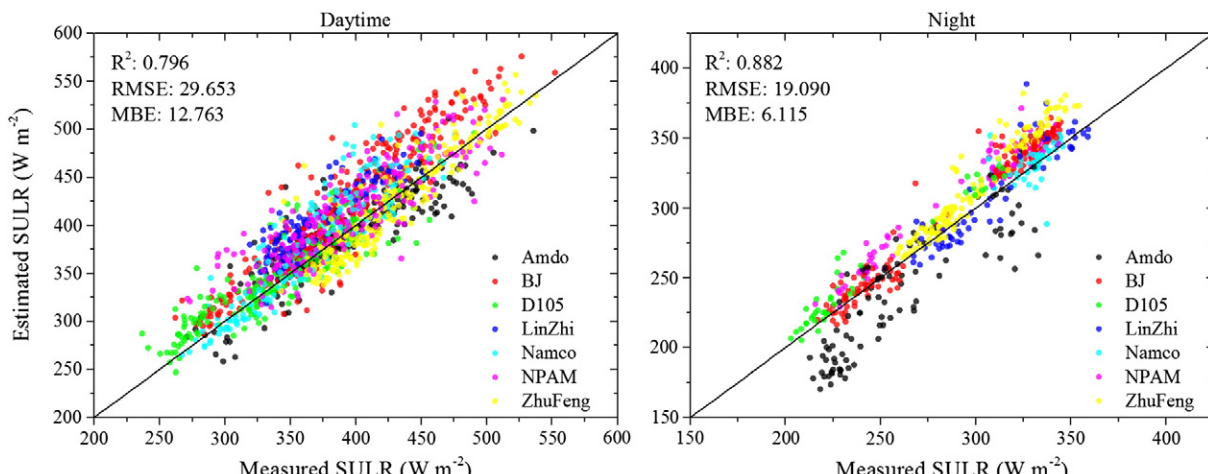


**Fig. 23.** The same results as that shown in Fig. 20 except the emphasis on the diurnal variation.

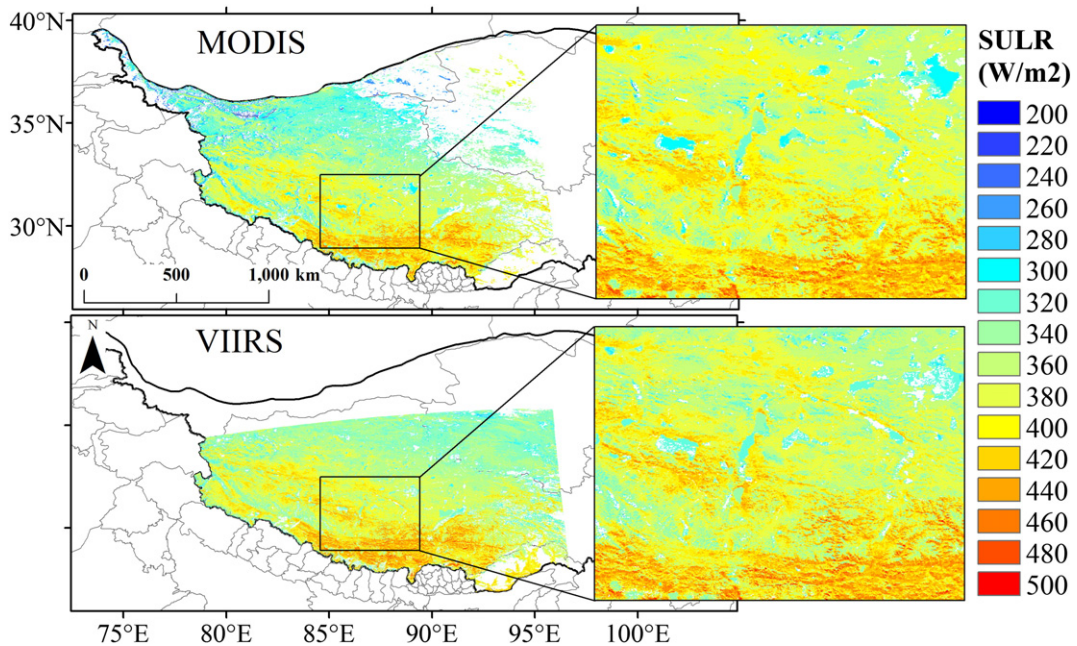


**Fig. 24.** The plots of SULR data derived from MODIS data (top) and VIIRS data (bottom). The bold black line indicates the boundary of the Tibetan Plateau. The gray lines are administrative boundary lines.

MODIS instrument, VIIRS can provide results as good as MODIS with 750 m finer resolution in the retrieval of SULR, and is a promising data source for retrieving surface radiation components and monitoring the surface energy balance.

The variable selection is a critical step in modeling SULR. Several analyses were performed, including variable selection based on the random forest method, sensitivity analyses of MODIS TOA radiances to the surface emissivity and temperature, variations of RMSEs of the ANN regression among different variable combinations, and the impact of view zenith angle on the ANN retrieval model. The results illustrate that TOA radiances of MODIS channels 29, 31, 32 and 33 (or VIIRS channels M14, M15 and M16) and VZA are sensitive to SULR, and they were selected as the input parameters in the ANN model.

Further sensitivity analyses were performed in order to check some issues concerning with in the course of modeling. The impact of the solar illumination on SULR was simulated with four typical cases of solar view zenith and relative azimuth angles based on statistical results within four months in the Tibetan Plateau. Results suggest that

differences with and without solar illumination are mainly focused on about 0.1% although the maximum can reach to circa 2%. Therefore, thermal model was chosen in the MODTRAN simulation due to the limited influence of the solar radiation. In addition, the profile quantity cannot significantly affect the regression accuracy of the ANN retrieval model as the mean RMSEs from about 11.1 to 11.5  $\text{W m}^{-2}$ . Consequently, the key factor is the representativeness of the atmosphere profile itself. Moreover, the influences of different spectral emissivities and emissivity data with various soil moistures on the ANN retrieval model were analyzed from the MODTRAN simulated dataset. It was found that the ANN model worked well for different emissivity data, and adapted to the impact of soil moisture on the emissivity.

A comprehensive and representative database is required to model SULR based on radiative transfer simulation and statistical model. Five criteria were used to screen the eligible air temperature and dew point temperature profiles from MODIS atmospheric profiles product. This procedure removed poor-quality profiles and ensured the representativeness of profile dataset in the Tibetan Plateau. And then in order to verify the reasonability of ANN interpolation, the statistical characteristics of main parameters in the simulated database were analyzed. TCPWV ranged from 0.01 to 4.489 cm with a mean of 0.532 cm. The elevation ranged from 0 to 6.53 km. The surface skin temperatures were between 220 and 340 K. The spatial distribution of profiles covered all possible surface types and was relatively concentrated along the boundary of the Tibetan Plateau. Lastly, all of the samples were evenly distributed across the whole year. Therefore, a reasonable simulation dataset was built for the ANN-based retrieval model.

The evaluation and comparison were performed firstly based on the simulation database. The validation by the training and testing database of both MODIS and VIIRS showed that ANN model is a good nonlinear model to fit SULR with the TOA radiances and VZA. The ANN model is preferred when comparing with the Wang2009 method using our simulation data. The ANN model can handle nonlinearity between SULR and TOA radiances better and produces better retrieval results with less RMSE and MBE.

Further, the MODIS-derived SULR values were validated using two-year ground measured data of seven stations in the Tibetan Plateau. The in situ measurements were first converted to SULR in spectral range of 4–100  $\mu\text{m}$  according to the fitted linear functions. The

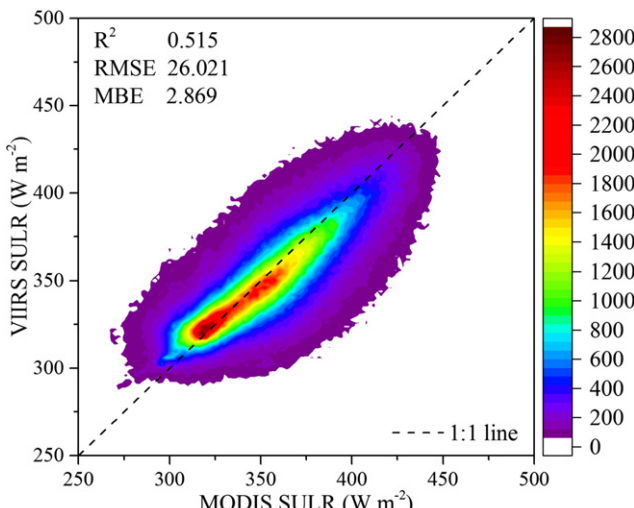


**Fig. 25.** The comparison of retrieved SULR from MODIS and VIIRS data.

evaluation results show that the  $R^2$ , RMSE and MBE are of 0.886, 26.985 W m $^{-2}$  and 10.812 W m $^{-2}$ , respectively. The seasonal differences between the samples were also analyzed, which indicated that this ANN-based hybrid method preferably models the seasonal variation of SULR. With respect to the validation of VIIRS-retrieved SULR, the discrepancy is relatively large when directly comparing VIIRS SULR with MODIS SULR. However, the overall trend and distribution are very similar. Most of the values are concentrated between 300 and 450 W m $^{-2}$  with  $R^2$  of 0.515, RMSE of 26.021 W m $^{-2}$  and MBE of 2.869 W m $^{-2}$ .

More ground measurements over different regions with various land covers are required for its further promotion. However, the surface heterogeneity and complicated terrain can lead to the difficulties in data matching and then influence the model's stability (Essery & Marks, 2007; Liang et al., 2002). In conclusion, although many refinements are envisioned, this approach is proved useful to retrieve the surface upward longwave radiation in an efficient way and provides source data for the research of the surface energy budget.

## Acknowledgments

This work has been supported by the state key program of Natural Science Foundation of China (NSFC) (Grant No. 41331171) and the National Key Basic Research Program of China (973 Program) (2013CB733402). The authors would like to thank NASA Goddard Space Flight Center (GSFC) Level 1 and Atmosphere Archive and Distribution System (LAADS) for providing us with the MODIS data products, the Comprehensive Large Array-data Stewardship System (CLASS) for providing VIIRS data products, the ASTER science team for providing the ASTER Spectral Library data, Dr. Zhengming Wan's Group at ICCESS (Institute for Computational Earth System Science) located on the campus of UCSB for releasing MODIS UCSB Emissivity Library, and Institute of Tibetan Plateau Research, Chinese Academy of Science for providing in situ radiation data at seven sites in the Tibetan Plateau. Besides, we wish to thank Dr. Heshun Wang (Institute of Remote Sensing and Digital Earth, Chinese Academy of Sciences) who provided us with the in situ emissivity data in different soil moisture conditions. Special thanks are also given to two anonymous reviewers for their valuable comments and suggestions that greatly improve this paper.

## References

- Abramowitz, G., Pouyanné, L., & Ajami, H. (2012). On the information content of surface meteorology for downward atmospheric long-wave radiation synthesis. *Geophysical Research Letters*, 39, L04808.
- Baldridge, A. M., Hook, S. J., Grove, C. I., & Rivera, G. (2009). The ASTER spectral library version 2.0. *Remote Sensing of Environment*, 113, 711–715.
- Barnes, W. L., Pagano, T. S., & Salomonson, V. V. (1998). Prelaunch characteristics of the Moderate Resolution Imaging Spectroradiometer (MODIS) on EOS-AM1. *IEEE Transactions on Geoscience and Remote Sensing*, 36, 1088–1100.
- Berk, A., Anderson, G. P., Acharya, P. K., Bernstein, L. S., Muratov, L., Lee, J., et al. (2006). MODTRAN5: 2006 update. 62331 F-62331F.
- Berk, A., Anderson, G. P., Bernstein, L. S., Acharya, P. K., Dothe, H., Matthew, M. W., et al. (1999). MODTRAN4 radiative transfer modeling for atmospheric correction. In A. M. Larar (Ed.), *Optical spectroscopic techniques and instrumentation for atmospheric and space research III* (pp. 348–353). Bellingham: Spie-Int Soc Optical Engineering.
- Breiman, L. (2001). Random forests. *Machine Learning*, 45, 5–32.
- Cao, C., Xiong, J., Blonski, S., Liu, Q., Upadhye, S., Shao, X., et al. (2013). Suomi NPP VIIRS sensor data record verification, validation, and long-term performance monitoring. *Journal of Geophysical Research, [Atmospheres]*, 118, 11664–11678.
- Diaz Uriarte, R., & Alvarez de Andres, S. (2006). Gene selection and classification of microarray data using random forest. *BMC Bioinformatics*, 7, 3.
- Ellingson, R. G. (1995). Surface longwave fluxes from satellite observations: a critical review. *Remote Sensing of Environment*, 51, 89–97.
- Essery, R., & Marks, D. (2007). Scaling and parametrization of clear-sky solar radiation over complex topography. *Journal of Geophysical Research, [Atmospheres]*, 112, D10122.
- Fairall, C. W., Persson, P. O. G., Bradley, E. F., Payne, R. E., & Anderson, S. P. (1998). A new look at calibration and use of Eppley precision infrared radiometers. Part I: theory and application. Part I: theory and application. *Journal of Atmospheric and Oceanic Technology*, 15, 1229–1242.
- Guan, H., Tremblay, A., Isaac, G. A., Strawbridge, K. B., & Banic, C. M. (2000). Numerical simulations of stratus clouds and their sensitivity to radiation—a RACE case study. *Journal of Applied Meteorology*, 39, 1881–1893.
- Gupta, S. K., Kratz, D. P., Wilber, A. C., & Nguyen, L. C. (2004). Validation of parameterized algorithms used to derive TRMM-CERES surface radiative fluxes. *Journal of Atmospheric and Oceanic Technology*, 21, 742–752.
- Helbig, N., & van Herwijnen, A. (2012). Modeling the spatial distribution of surface hoar in complex topography. *Cold Regions Science and Technology*, 82, 68–74.
- Huang, G., Liu, S., & Liang, S. (2011). Estimation of net surface shortwave radiation from MODIS data. *International Journal of Remote Sensing*, 33, 804–825.
- Hulley, G. C., Hook, S. J., & Baldridge, A. M. (2010). Investigating the effects of soil moisture on thermal infrared land surface temperature and emissivity using satellite retrievals and laboratory measurements. *Remote Sensing of Environment*, 114, 1480–1493.
- Hutchison, K. D., Isager, B. D., & Hauss, B. (2011). The use of global synthetic data for pre-launch tuning of the VIIRS cloud mask algorithm. *International Journal of Remote Sensing*, 33, 1400–1423.
- Kato, S., Loeb, N. G., Rose, F. G., Doelling, D. R., Rutan, D. A., Caldwell, T. E., et al. (2013). Surface irradiances consistent with CERES-derived top-of-atmosphere shortwave and longwave irradiances. *Journal of Climate*, 26, 2719–2740.
- Kim, B. J. (2004). Performance of networks of artificial neurons: the role of clustering. *Physical Review E*, 69, 4.
- Krasnopolsky, V. M., Fox-Rabinovitz, M. S., & Chalikov, D. V. (2005). New approach to calculation of atmospheric model physics: accurate and fast neural network emulation of longwave radiation in a climate model. *Monthly Weather Review*, 133, 1370–1383.
- Liang, S., Fang, H., Chen, M., Shuey, C. J., Walther, C., Daughtry, C., et al. (2002). Validating MODIS land surface reflectance and albedo products: methods and preliminary results. *Remote Sensing of Environment*, 83, 149–162.
- Lipton, A. E. (1992). Effects of slope and aspect variations on satellite surface temperature retrievals and mesoscale analysis in mountainous terrain. *Journal of Applied Meteorology*, 31, 255–264.
- Lipton, A. E., & Ward, J. M. (1997). Satellite-view biases in retrieved surface temperatures in mountain areas. *Remote Sensing of Environment*, 60, 92–100.
- Liu, Y., Hiyama, T., & Yamaguchi, Y. (2006). Scaling of land surface temperature using satellite data: a case examination on ASTER and MODIS products over a heterogeneous terrain area. *Remote Sensing of Environment*, 105, 115–128.
- Long, D., Gao, Y., & Singh, V. P. (2010). Estimation of daily average net radiation from MODIS data and DEM over the Baiyangdian watershed in North China for clear sky days. *Journal of Hydrology*, 388, 217–233.
- Manners, J., Vosper, S. B., & Roberts, N. (2012). Radiative transfer over resolved topographic features for high-resolution weather prediction. *Quarterly Journal of the Royal Meteorological Society*, 138, 720–733.
- Masson, V., Champeaux, J.-L., Chauvin, F., Meriguet, C., & Lacaze, R. (2003). A global database of land surface parameters at 1-km resolution in meteorological and climate models. *Journal of Climate*, 16, 1261–1282.
- Michel, D., Philippon, R., Ruckstuhl, C., Vogt, R., & Vuilleumier, L. (2008). Performance and uncertainty of CNR1 net radiometers during a one-year field comparison. *Journal of Atmospheric and Oceanic Technology*, 25, 442–451.
- Mira, M., Valor, E., Boluda, R., Caselles, V., & Coll, C. (2007). Influence of soil water content on the thermal infrared emissivity of bare soils: implication for land surface temperature determination. *Journal of Geophysical Research, Earth Surface*, 112, F04003.
- Mira, M., Valor, E., Caselles, V., Rubio, E., Coll, C., Galve, J. M., et al. (2010). Soil moisture effect on thermal infrared (8–13-μm) Emissivity. *IEEE Transactions on Geoscience and Remote Sensing*, 48, 2251–2260.
- Mlyniczak, P. E., Smith, G. L., Wilber, A. C., & Stackhouse, P. W. (2011). Annual cycle of surface longwave radiation. *Journal of Applied Meteorology and Climatology*, 50, 1212–1224.
- Naud, C. M., Chen, Y., Rangwala, I., & Miller, J. R. (2013). Sensitivity of downward longwave surface radiation to moisture and cloud changes in a high-elevation region. *Journal of Geophysical Research, [Atmospheres]*, 118, 10072–10081.
- Nussbaumer, E. A., & Pinker, R. T. (2012). Estimating surface longwave radiative fluxes from satellites utilizing artificial neural networks. *Journal of Geophysical Research, [Atmospheres]*, 117, D07209.
- Oliphant, A. J., Spronken-Smith, R. A., Sturman, A. P., & Owens, I. F. (2003). Spatial variability of surface radiation fluxes in mountainous terrain. *Journal of Applied Meteorology*, 42, 113–128.
- Pinker, R. T., & Laszlo, I. (1992). Modeling surface solar irradiance for satellite applications on a global scale. *Journal of Applied Meteorology*, 31, 194–211.
- Qiu, J. (2008). The third pole. *Nature*, 454, 393–396.
- Ren, Liang, S., Yan, G., & Cheng, J. (2013). Empirical algorithms to map global broadband emissivities over vegetated surfaces. *IEEE Transactions on Geoscience and Remote Sensing*, 51, 2619–2631.
- Ren, H., Rongyan, L., Guangjian, Y., Xihan, M., Zhao-Liang, L., Nerry, F., et al. (2014). Angular normalization of land surface temperature and emissivity using multiangular middle and thermal infrared data. *IEEE Transactions on Geoscience and Remote Sensing*, 52, 4913–4931.
- Ren, H., Yan, G., Chen, L., & Li, Z. (2011). Angular effect of MODIS emissivity products and its application to the split-window algorithm. *ISPRS Journal of Photogrammetry and Remote Sensing*, 66, 498–507.
- Rubio, E., Caselles, V., & Badenas, C. (1997). Emissivity measurements of several soils and vegetation types in the 8–14 μm waveband: analysis of two field methods. *Remote Sensing of Environment*, 59, 490–521.
- Schulz, J., Albert, P., Behr, H. D., Capriotti, D., Deneke, H., Dewitte, S., et al. (2009). Operational climate monitoring from space: the EUMETSAT Satellite Application Facility on Climate Monitoring (CM-SAF). *Atmospheric Chemistry and Physics*, 9, 1687–1709.
- Seemann, S. W., Li, J., Menzel, W. P., & Gumley, L. E. (2003). Operational retrieval of atmospheric temperature, moisture, and ozone from MODIS infrared radiances. *Journal of Applied Meteorology*, 42, 1072–1091.

- Senkova, A. V., Rontu, L., & Savijärvi, H. (2007). Parametrization of orographic effects on surface radiation in HIRLAM. *Tellus A*, 59, 279–291.
- Sharma, N., & Ali, M. M. (2013). A neural network approach to improve the vertical resolution of atmospheric temperature profiles from geostationary satellites. *IEEE Geoscience and Remote Sensing Letters*, 10, 34–37.
- Shi, Q., & Liang, S. (2013). Characterizing the surface radiation budget over the Tibetan Plateau with ground-measured, reanalysis, and remote sensing data sets: 2. Spatio-temporal analysis. *Journal of Geophysical Research, [Atmospheres]*, 118, 8921–8934.
- Soci, C., Fischer, C., & Horányi, A. (2006). Sensitivity of high-resolution forecasts using the adjoint technique at the 10-km scale. *Monthly Weather Review*, 134, 772–790.
- Stephens, G. L., Wild, M., Stackhouse, P. W., L'Ecuyer, T., Kato, S., & Henderson, D. S. (2012). The global character of the flux of downward longwave radiation. *Journal of Climate*, 25, 2329–2340.
- Strobl, C., Boulesteix, A. -L., Zeileis, A., & Hothorn, T. (2007). Bias in random forest variable importance measures: illustrations, sources and a solution. *BMC Bioinformatics*, 8, 25.
- Tang, B., & Li, Z. -L. (2008). Estimation of instantaneous net surface longwave radiation from MODIS cloud-free data. *Remote Sensing of Environment*, 112, 3482–3492.
- Wang, K., & Liang, S. (2009). Evaluation of ASTER and MODIS land surface temperature and emissivity products using long-term surface longwave radiation observations at SURFRAD sites. *Remote Sensing of Environment*, 113, 1556–1565.
- Wang, W., & Liang, S. (2010). A method for estimating clear-sky instantaneous land-surface longwave radiation with GOES sounder and GOES-R ABI data. *IEEE Geoscience and Remote Sensing Letters*, 7, 708–712.
- Wang, W., Liang, S., & Augustine, J. A. (2009). Estimating high spatial resolution clear-sky land surface upwelling longwave radiation from MODIS data. *IEEE Transactions on Geoscience and Remote Sensing*, 47, 1559–1570.
- Wang, K., Wan, Z., Wang, P., Sparrow, M., Liu, J., Zhou, X., et al. (2005). Estimation of surface long wave radiation and broadband emissivity using Moderate Resolution Imaging Spectroradiometer (MODIS) land surface temperature/emissivity products. *Journal of Geophysical Research, [Atmospheres]*, 110, D11109.
- Wang, T., Yan, G., & Chen, L. (2012). Consistent retrieval methods to estimate land surface shortwave and longwave radiative flux components under clear-sky conditions. *Remote Sensing of Environment*, 124, 61–71.
- Wonsick, M. M., & Pinker, R. T. (2013). The radiative environment of the Tibetan Plateau. *International Journal of Climatology*, 34, 2153–2162.
- Xiao, Q., Liu, Q. H., Li, X. W., Chen, L. F., Liu, Q., & Xin, X. Z. (2003). A field measurement method of spectral emissivity and research on the feature of soil thermal infrared emissivity. *Journal of Infrared and Millimeter Waves*, 22, 373–378.
- Yang, K., Koike, T., Stackhouse, P., Mikovitz, C., & Cox, S. J. (2006). An assessment of satellite surface radiation products for highlands with Tibet instrumental data. *Geophysical Research Letters*, 33, L22403.
- Yang, K., Wu, H., Qin, J., Lin, C., Tang, W., & Chen, Y. (2014). Recent climate changes over the Tibetan Plateau and their impacts on energy and water cycle: a review. *Global and Planetary Change*, 112, 79–91.
- Zhang, Y., Rossow, W. B., Lacis, A. A., Oinas, V., & Mishchenko, M. I. (2004). Calculation of radiative fluxes from the surface to top of atmosphere based on ISCCP and other global data sets: refinements of the radiative transfer model and the input data. *Journal of Geophysical Research, [Atmospheres]*, 109, D19105.
- Zhang, Y., Rossow, W. B., & Stackhouse, P. W., Jr. (2007). Comparison of different global information sources used in surface radiative flux calculation: radiative properties of the surface. *Journal of Geophysical Research, [Atmospheres]*, 112, D01102.
- Zhang, Y., Wang, D., Zhai, P., Gu, G., & He, J. (2013). Spatial distributions and seasonal variations of tropospheric water vapor content over the Tibetan Plateau. *Journal of Climate*, 26, 5637–5654.